



## Wide-angle seismic imaging of divergent and transform segments of the Pará-Maranhão-Barreirinhas-Ceará margin, NW Brazil

Philippe Schnürle<sup>a,\*</sup>, Flora Gallais<sup>a</sup>, Alexandra Afilhado<sup>b,c</sup>, Maryline Moulin<sup>a</sup>, Nuno Dias<sup>b,c</sup>, José Soares<sup>d</sup>, Afonso Loureiro<sup>b,c</sup>, Reinhardt Fuck<sup>d</sup>, José Antonio Cupertino<sup>e</sup>, Adriano Viana<sup>e</sup>, Daniel Aslanian<sup>a</sup>, Magic Team

<sup>a</sup> Geo-Ocean, Univ Brest, CNRS, Ifremer, UMR6538, F-29280, Plouzane, France

<sup>b</sup> Instituto Dom Luis (IDL), Faculdade de Ciências da Universidade de Lisboa, 1749-016, Lisboa, Portugal

<sup>c</sup> Instituto Superior de Engenharia de Lisboa (ISEL), Rue Conselheiro Emídio Navarro, 1959-007, Lisboa, Portugal

<sup>d</sup> Lablithos, Instituto de Geociências (IG), Universidade de Brasília, Campus Darcy Ribeiro, 70910- 900, Brasília, Brazil

<sup>e</sup> PETROBRAS/CENPES-PROFEX, Rio de Janeiro, Brazil

### ARTICLE INFO

#### Keywords:

North-east equatorial Brazil  
Transform Margin  
Deep seismic structure

### ABSTRACT

The structure of the North-East equatorial Brazilian margin was investigated during the MAGIC (Margins of Brazil, Ghana and Ivory Coast) seismic wide-angle experiment. This study focuses on the MC5 profile, that spans NW-SE 720 km in length, from the São Paulo Double Fracture Zone to the Barreirinhas margin and continental Borborema province. Its main objective is to understand the fundamental processes which lead to the thinning and finally to the breakup of the continental crust in a specific context of a divergent pull-apart system with two strike-slip borders. The experiment was devised to obtain the 2D structure along this profiles from joint pre-stack depth migration of streamer data and travel-time inversion by forward modeling of 43 Ocean Bottom Seismometers and 21 Land Seismic Stations records. Along the MC5 wide-angle transect, 4 major sectors are identified: 1) the São Paulo Double Fracture Zone presenting a 4.5 km thick volcano-sedimentary Basin on top of a 5.5 km thick basement; 2) a volcanic alignment and intermediate domain SE-ward, formed by the 4.5 km thick Basin III; 3) the 7.5 km thick Basin II, and the 5.5 km thick Basin I composing the continental slope and shelf. While all the offshore basement remains about 6 km thick in the deep-sea domains, acoustic velocity evolves from two-layer 4.8–6 km/s and 6.1–6.8 km/s beneath Basin III to two-layer high velocity 6.1–6.8 km/s and 7.2–7.4 km/s beneath Basin II and I. The necking zone, forming the Parnaíba Platform and associated Piauí-Camocim and Ceará Basins, is 50 km wide; 4) the Médio Coreáú and Ceará Central thrust belt, where the unthinned continental crust thickness reaches 32 km. Finally, a schematic kinematic reconstruction that satisfies these observation is argued.

### 1. Introduction

The Equatorial Atlantic ocean is separated from the Central Atlantic Ocean, to the north, by the Guinea Fracture Zone and, to the south, from the South Atlantic Ocean by the Chain Fracture Zone (Campan, 1995; Basile et al., 2005). The ocean spans NS-ward 2000 km in length and can be divided into three 600–800 km long major sub-segments, separated by main fracture zones (Moulin et al., 2010, Fig. 1). The northern segment is bounded by the Sierra Leone Fracture Zone to the north and

the São Paulo double Fracture Zone (SPdFZ) to the south and consist in two ~400 km-large segments separated by the 4°N Fracture Zone and fringed by the Demerara plateau-Sierra Leone conjugate passive margins system and the Foz do Amazonas-Liberian conjugate passive margins system. The central segment is bounded by the Sao Paulo double Fracture Zone to the north and the Chain Fracture Zone (CFZ). It comprises 2 segments, about 300 km wide: the Ceará-Potiguar and the East Ghana basin-Togo-Benue conjugate passive margins system and the Pará-Maranhão-Barreirinhas and the Deep Ivory Basin-Ghana conjugate

Given their role as Guest Editor, Anderson Santos and Eduardo Rocha-Júnior were not involved in the peer-review of this article and had no access to information regarding its peer-review. Full responsibility for the editorial process for this article was delegated to Journal Editor Andrés Folguera.

\* Corresponding author.

E-mail address: [philippe.schnurle@ifremer.fr](mailto:philippe.schnurle@ifremer.fr) (P. Schnürle).

<https://doi.org/10.1016/j.jsames.2023.104394>

Received 14 March 2023; Received in revised form 1 May 2023; Accepted 2 May 2023

Available online 4 May 2023

0895-9811/© 2023 Elsevier Ltd. All rights reserved.

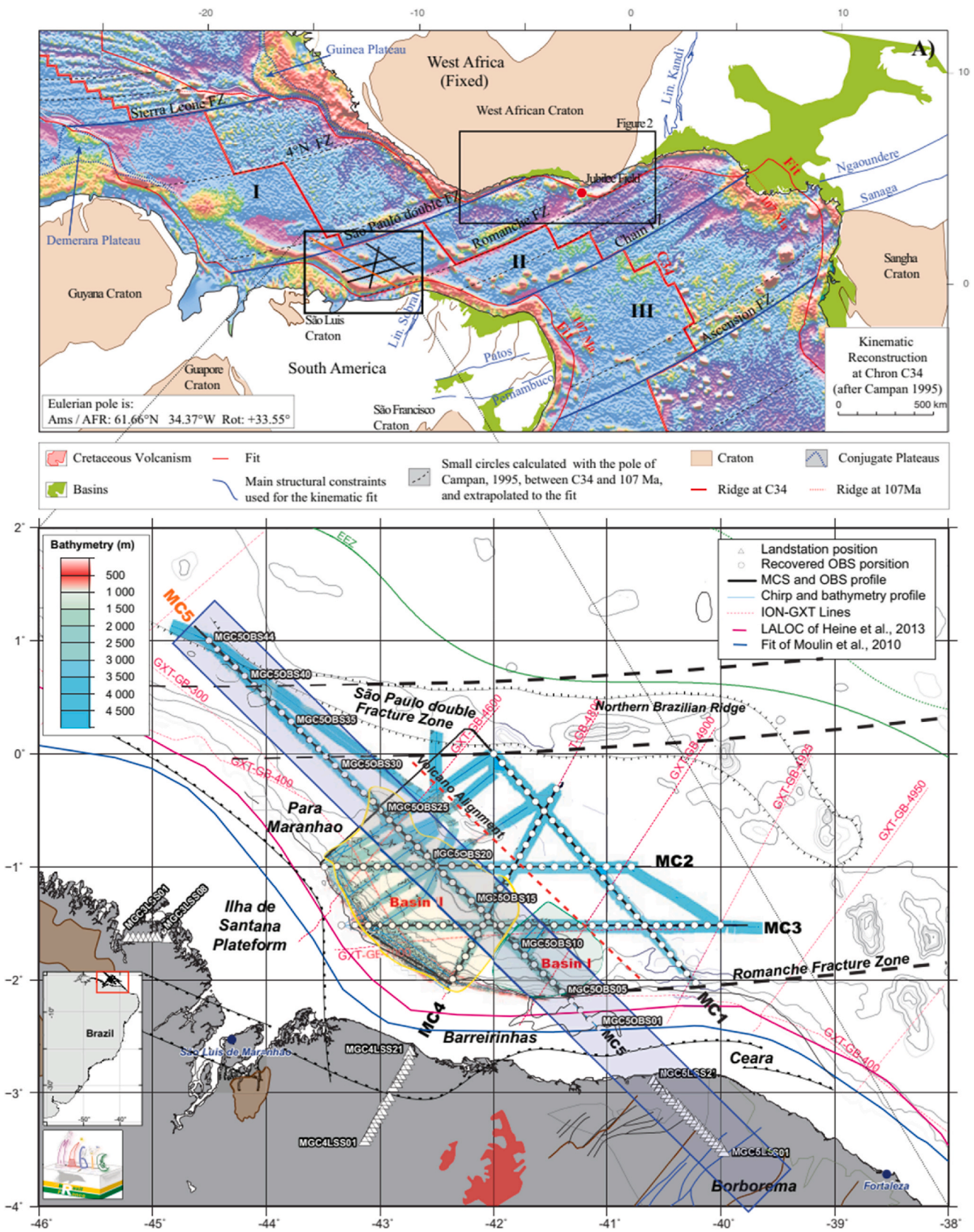
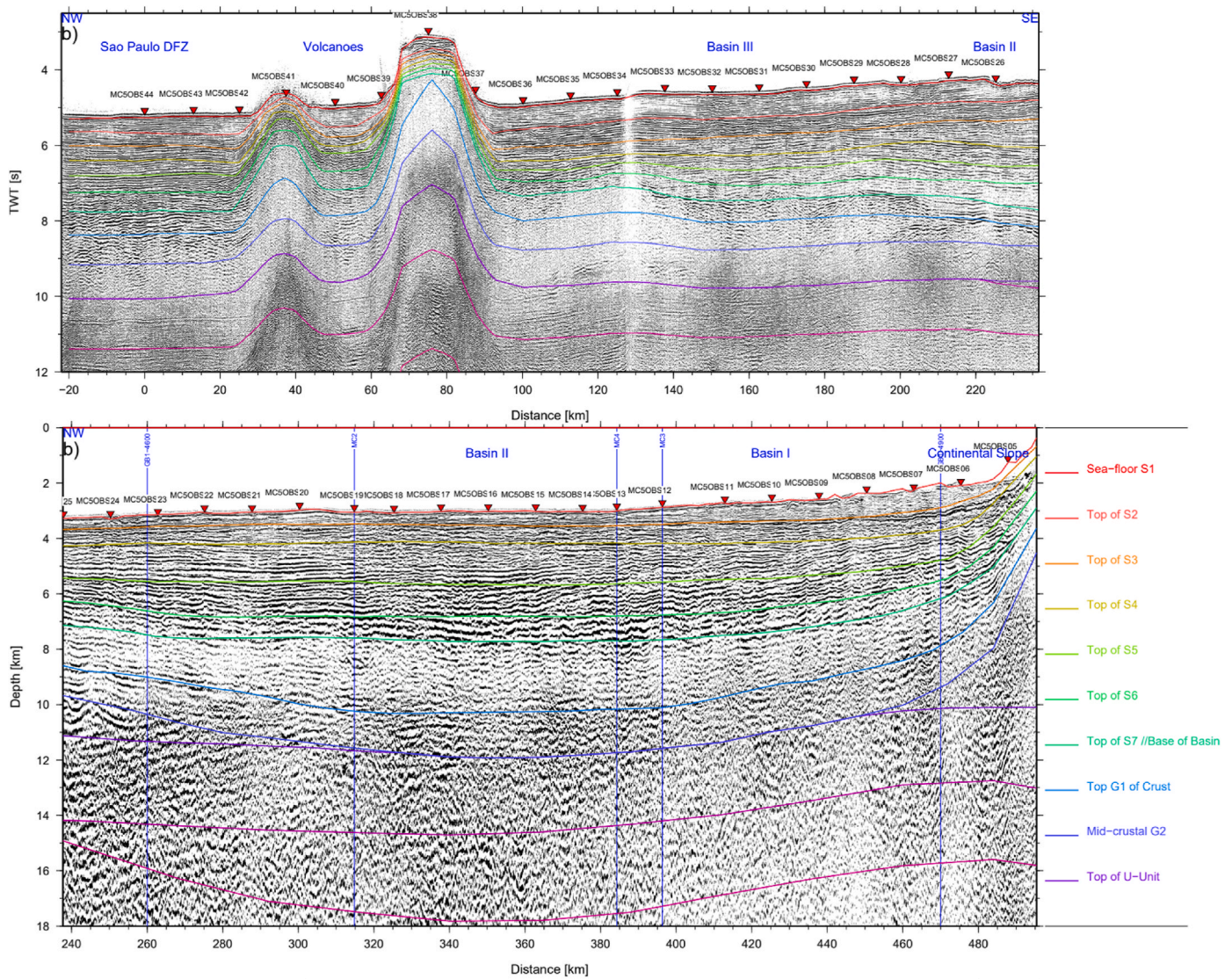


Fig. 1. a) Kinematic reconstruction at C34 (Campanian, 84 Ma), after [Moulin et al. \(2010\)](#), showing the segmentation of the of the Equatorial Atlantic Ocean, b) Location map of the MAGIC experiment. The OBS and the land stations are presented by white circles and triangles, respectively. Available industrial seismic refraction profiles of Ion -GXT are represented in red. The swath bathymetric data of the survey is underlain.



**Fig. 2.** Two-way travel-time record section of MCS data along MC5 profile overlain by time converted interfaces of the wide-angle model represented with continuous lines. a) Western part across the SPDFZ and Basin III. b) Eastern part across Basin II and I. The intersections with the MAGIC and the ION GXT dataset are indicated blue vertical lines. OBS location are indicated by red inverted triangles. Vertical exaggeration at seafloor is 1:12.5.

passive margins system separated by the Romanche Fracture Zone (RFZ). The SPDFZ, RFZ and CFZ have offset magnitude of about 600, 920 and 320 Km, respectively (de Matos and Brown, 1992; Tavares et al., 2020). The RFZ can be traced 3200 km from South America to West Africa and is the second longest fracture zone in the world (Francheteau and Le Pichon, 1972; Gorini, 1977). Thus, the breakup of northwestern Gondwana occurred in a sequence of several distinct pull-apart basins connected by strike-slip/transform faults in three Mesozoic extensional events (Davison et al., 2015). Hence, a trans-tensional shear corridor with dextral sense of displacement was developed along the present-day northern, equatorial continental margin of Brazil, which formed the Pará-Maranhão and Barreirinhas marginal basins (e.g. de Matos et al., 2021; de Castro et al., 2022).

The structure of the North-East equatorial Brazilian margin was investigated during the MAGIC (Margins of Brazil, Ghana and Ivory Coast) seismic experiment, a project conducted by IFREMER (Institut Français de Recherche pour l'Exploration de la Mer), UnB (University of Brasília), FCUL (Faculdade de Ciências da Universidade de Lisboa) and Petrobras. The survey consists of 5 deep seismic profiles totaling 1900 km of marine multi-channel seismic reflection (MCS) and wide angle acquisition with 143 deployments of short-period Ocean Bottom

Seismometers (OBS) from the IFREMER pool. Three of the profiles were extended into land using Land Seismic Stations (LSS) from the Brazilian pool at a total of 50 points. This study focuses on the MC5 wide-angle profile, that spans NW-SE offshore from the São Paulo double Fracture Zone to the Borborema-Ceará margin onshore. Its main objective is to understand the fundamental processes which lead to the thinning and finally to the breakup of the continental crust in a specific context of a pull-apart system with two strike-slip borders. The experiment was devised to obtain the 2D structure along the profiles from joint pre-stack depth migration of the reflection streamer data together with forward modeling of the OBS/LSS records.

## 2. Data and method

The MC5 profile is a 720 km long wide-angle transect that spans NW-SE from the SPDFZ to the continental Borborema province (Fig. 1). The profile runs rather parallel to the Ilha de Santana Platform until near MCSOBS15, then nearly 45° oblique to the Barreirinhas -Borborema continental slope and shelf. At sea, a total of 44 OBS were planned (MCSOBS43 was not deployed), spaced every 7 nmi (~13 km). MC5 extends 150 km on land towards the ESE, in the Borborema area, by the

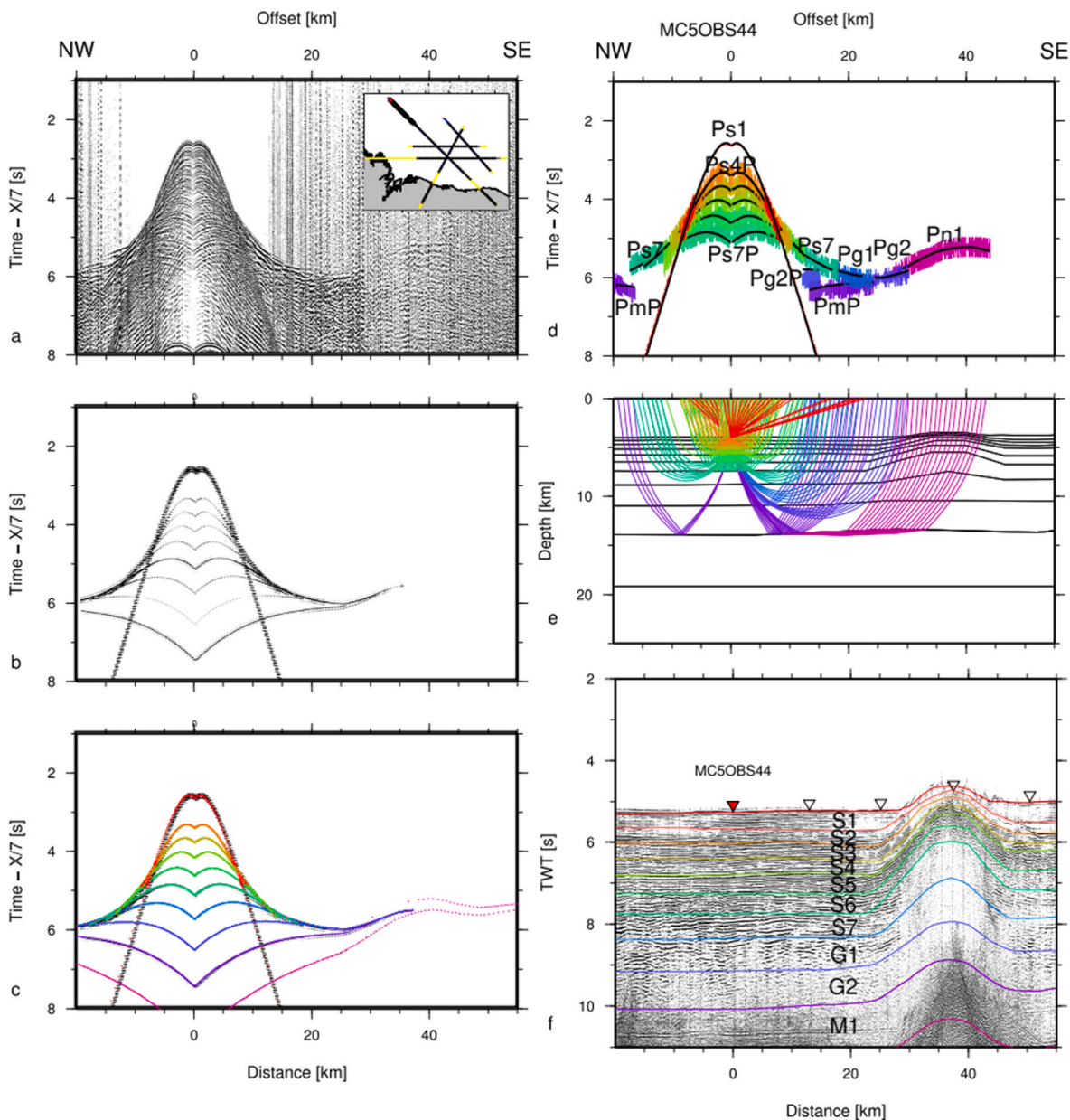


**Fig. 3.** MC5OBS44 on profile MC5 in the SPdFZ. a) Seismic record; b) Synthetics. c) Color coded synthetics. d) Color-coded observed travel-times overlain by predicted times in black. e) Seismic rays. f) MCS time migrated section and color-coded model interfaces. On a, b, c, and d, travel-time is reduced by a velocity of 7 km/s.

deployments of 21 arrays of LSS. Shots were acquired together with streamer data from MC5OBS44 until MC5OBS05 were water depth shallows to less than 100 m. Thus on the shelf, no shots nor streamer data were acquired from MC5OBS04 to MC5OBS01.

### 2.1. Seismic reflection data

Along the MAGIC MC5 wide-angle transect, 6 major sectors are identified: 1) the deep sea Basin in the SPdFZ, 3) the volcanic line to the SW of southern SPdFZ, 3) the intermediate Basin III, 4) the Basin II principal focus of the MAGIC survey, 5) the Basin I composing the continental slope, the Parnaíba Platform and associated Piauí-Camocim and Ceará Basins, 6) and finally the Médio Coreaú and Ceará Central thrust belt. In the seismic profile (Fig. 2), we identify 7 well stratified layers down to 9 s twt (marked with rainbow colors ranging from red to green) on top of 2 layers (marked in blue). The S7 unit and underlying basement is characterized by discontinuous events of nearly transparent

and high amplitude series about 10–20 km wide and 0.5–1 s twt thick. Seismic imaging across the volcanoes is poor owing to the steeply dipping reflectors and the possible mixed magmatic and sedimentary complex that composes the core and flanks of the volcanoes (Fig. 2 between 15 and 100 km).

Toward the southeast in Basin III between 100 and 220 km profile distance, the 1 s twt thick S1 and S2 sedimentary units are well preserved, while S3, S4, S5 and S6 units thicken from less than 1–2.25 s twt on top of the southeastward dipping. Basin II presents a very sharp amplitude contrast at the base of S5 unit (Fig. 2 between 240 and 410 km). However all units appear to constitute a 250 km wide synclinal basin with its axis located near 360 km model distance and extending to the foot of the continental slope at the SE extremity of MC5MCS profile. In Basin II, S1 to S5 units a relatively flat, continuous and isopach sequence lying between 4 and 7 s twt. In Basin I, this sequence thins down to less than 3 s twt at the continental slope and is associated to more chaotic seismic events probably related to mass transport deposit

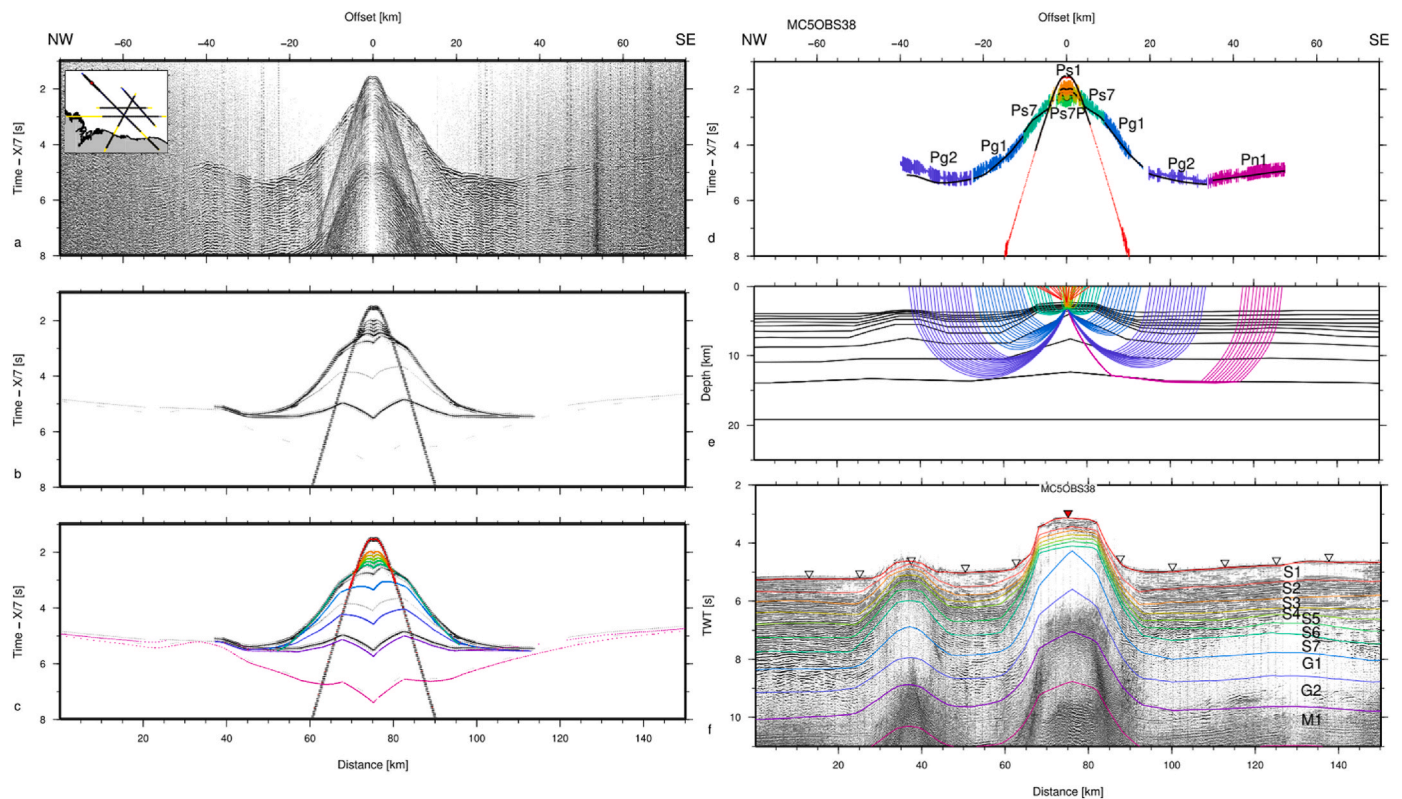


**Fig. 4.** MC5OBS38 on profile MC5 at the top of the volcano in the SPdFZ. a) Seismic record. b) Synthetics. c) Color coded synthetics. d) Color-coded observed travel-times overlain by predicted times in black. e) Seismic rays. f) MCS time migrated section and color-coded model interfaces. On a, b, c, and d, travel-time is reduced by a velocity of 7 km/s.

and submarine channel migrations (Fig. 2 between 410 and 495 km). The following paragraph contains the description of the OBS seismic records (as well as synthetics), the interpreted travel times together with their predicted counterpart, along the 5 different transects of the wide angle MC5 profile.

## 2.2. Wide-angle data

### 2.2.1. The São Paulo double fracture zone

In the SPdFZ, between 7.5 and 8.5 km depth (S7), a sequences of bright pre-critical reflections Ps7P are observed on the MCS and OBS data, together with refraction Ps7 presenting apparent velocities increasing from 4.2 to 4.8 km/s between 7 and 15 km offset. Then two refracted events Pg1 and Pg2 are observed between 10 and 30 km offset as high amplitude first arrivals (Fig. 3, blue and dark blue) with apparent velocity increasing from 5.0 to 6.8 km/s. Turning waves from the upper-mantle (Pn1 arrivals in magenta) can be identified between 25 and 40 km offset, suggesting that the Moho at the WNW limit of MC5 profile is located near 14 km depth. Velocity in the lithospheric mantle increases from 7.9 to 8.15 within 5 km depth.

The velocity structure of the volcanic edifices located SE-ward of the SPdFZ is best identified from MC5OBS38 located on top of the main volcano (Fig. 4): velocity increases from 2.1 to 4.2 km/s from about 2.5 to 3.75 km depth (S1 to S6) accompanied by about 750 ms twt bright acoustic reflections on MC5OBS38 and MC5MCS (Fig. 2). The Ps6 departs from earlier refractions as a sharp high velocity event, indicating a contrast between the top and flanks of the volcano and its chimney at the core of the volcano. The Moho remains close to 14 km depth.

### 2.2.2. The basin III

The model structure appears to be preserved SW-ward of the SPdFZ across the magmatic domain and into Basin III. In layer S5 and S6, high

amplitude discontinuous reflections are observed on the MC5MCS profile, similar to those imaged between -20 and 20 km model distance, suggesting again volcano-sedimentary deposits characterized by relatively low velocities of less than 4 km/s. Velocity increases from 4.2 to 4.8 in layer S7. Bright refracted Pg1 and Pg2 events between 15 and 40 km offset arise from within layer G1 and G2. In this area, the basement velocity varies slightly from one OBS to another but an approximately 14 km deep Moho appears to prevails, based on PmP and Pn1 arrivals. Reflections from within the mantle are also observed (Fig. 5).

### 2.2.3. The basin II

From model distance 190 km near MC5OBS29, the high amplitude discontinuous reflections are not present on the MCS profile (Fig. 2), suggesting that volcano-sedimentary deposit does not extend SE-ward. The basin's sedimentary units thicken, particularly S3, S4 and S6 until 350 km near MC5OBS16. From 260 km, the reflexions becomes discontinuous at S5: a bright reflection Ps5P (in light green) and associated high apparent velocity (up to 4.8 km/s) refraction Ps5 (in olive green) becomes more prominent (at MC5OBS19, Fig. 6). Below, the velocity return to a sedimentary basin trend: this velocity inversion results in refracted events Ps6 and Ps7, of 4.2–4.6 km/s apparent velocity, that arrive as secondary arrivals and that are mixed with the high amplitude events arising from the crust and the PmP reflection at the Moho. Only below 9 km depth, Pg1 and Pu refractions from layer 8 and 9 indicate crustal velocities exceeding 5.2 km/s. On MC5MCS, the seismic amplitude decreases within S5, and events from within S6 and S7 remain weak and very noisy. Therefore, the top of the acoustic basement in Basin II remains somewhat uncertain.

Below Basin II, Pn1 refractions in the upper mantle are preceded by a branch Pu of relatively high amplitude and approximately 7.5 km/s apparent velocity (from about 20 up to 45 km offset on MC5OBS13, Fig. 7) and from 20 to 35 km offset on MC5OBS12 to MC5OBS06 (Fig. 8)

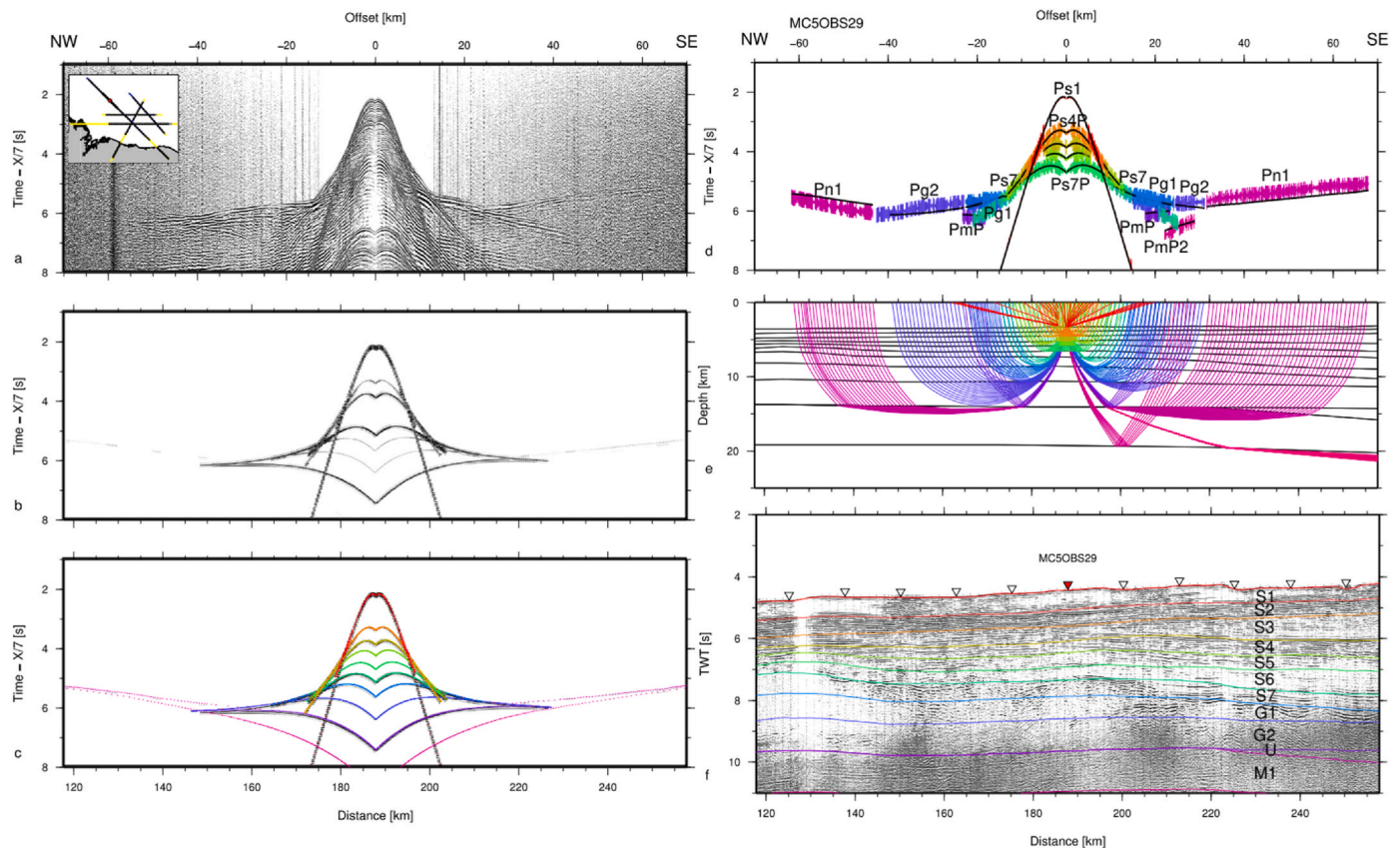


**Fig. 5.** MC5OBS29 on profile MC5 in the Basin III. a) Seismic record. b) Synthetics. c) Color coded synthetics. d) Color-coded observed travel-times overlain by predicted times in black. e) Seismic rays. f) MCS time migrated section and color-coded model interfaces. On a, b, c, and d, travel-time is reduced by a velocity of 7 km/s.

followed by a Pn1 of relatively weak amplitude and fast apparent velocity (from about 40 up to 45 km offset). Several reflections are observed as PuP and PmP.

#### 2.2.4. The basin I and the continental slope

The thickness of the sedimentary basin at the foot of the continental slope decreases to 5 km on the MC5MCS profile and OBS records become very asymmetric (Figs. 2 and 8). The data quality on the 5 OBS located in the slope and on the continental shelf decreases when compared to those located in the deep sea basin. The recorded sedimentary and crustal events suggest that this thickness about 5 km of Basin I is preserved until at least MC5OBS01. Pg1, Pu, and Pn1 events allow good constrain of the margin's crustal velocity and thickness. In this area the Moho remains near 14 km depth, but appears to dive at 510 km model distance (to 16 km when considering records from MC5OBS01).

#### 2.2.5. The barreirinhas-borborema margin

Refracted events in the continental crust (Pg2 in blue) and reflected events at its base (PmP in dark blue) are relatively strong on the land stations located closer to the coastline, as shown on MC5LSS21 located at 612 km model-distance, between 100 and 150 km offset for instance (Fig. 9). On MC5LSS01 located 100 km landward at 712 km model-distance, Pg2 and PmP have weaker amplitude but a good travel-time fit (Fig. 10). When looking at LSS seaward, the travel-time gap between Pg2 and PmP increases as long as the Moho remains deep since the Pg ray paths becomes shorter and shallower when compared to PmP ray-path. This gap decreases when the Moho rises over the necking area of crustal thinning. These crustal arrivals are preceded by Pn1 first-arrivals propagating deep in the upper mantle down to 50 km depth and are recorded with significant energy up to 600–700 km offset. The

apparent velocity of the Pn1 arrival increases between model distance 440–420, then decreases until 350 km where the Pn1 amplitude is weak. It increases again between 325 and 180 km accompanied by strong amplitude. A 3rd segment of Pn1 arrivals is observed from shots at the SPDFZ near 700–600 km model distance. The fact the Pn1 amplitude and apparent velocity variations are dependant on the model-distance rather than the offset implies that the mantle velocity varies both with depth and along the model. We have, at this stage, introduced a mantelic stratification that is able to fit reasonably well the first arrivals up to 720 km model distance.

### 3. Velocity model

The final velocity model is 60 km deep and 720 km long, including 550 km offshore and 170 km onshore. The model consists of 14 layers. For the sedimentary layers up to the basement, the interface geometry is well constrained in twt from the MCS data. Thus, a short interface node spacing is selected (between 2 km at the sea-floor and 8 km for the deepest layer) and a sequence of dumped least squares inversion on the velocity (Zelt and Smith, 1992) and recalculating the depths is performed up to get an appropriate fit of the arrival times. The gradients of the layers are then controlled by amplitude modeling. In order to model the lateral variations of the seismic velocity with sufficient resolution, velocity nodes are spaced by 24 km in the shallow layers S1 to S5, then by 48 km). In the basement and mantle, the interface nodes are wider apart: between 8 and 12 km in the basement, and 48 km in the mantle. The velocity nodes in the basement are spaced by 48 km, and in the mantle by 720 km, i.e. one node at each extremity. Then, the depth of the interface nodes together with both the top velocity and velocity gradient are inverted in the remaining layers (L5 to L14), with the

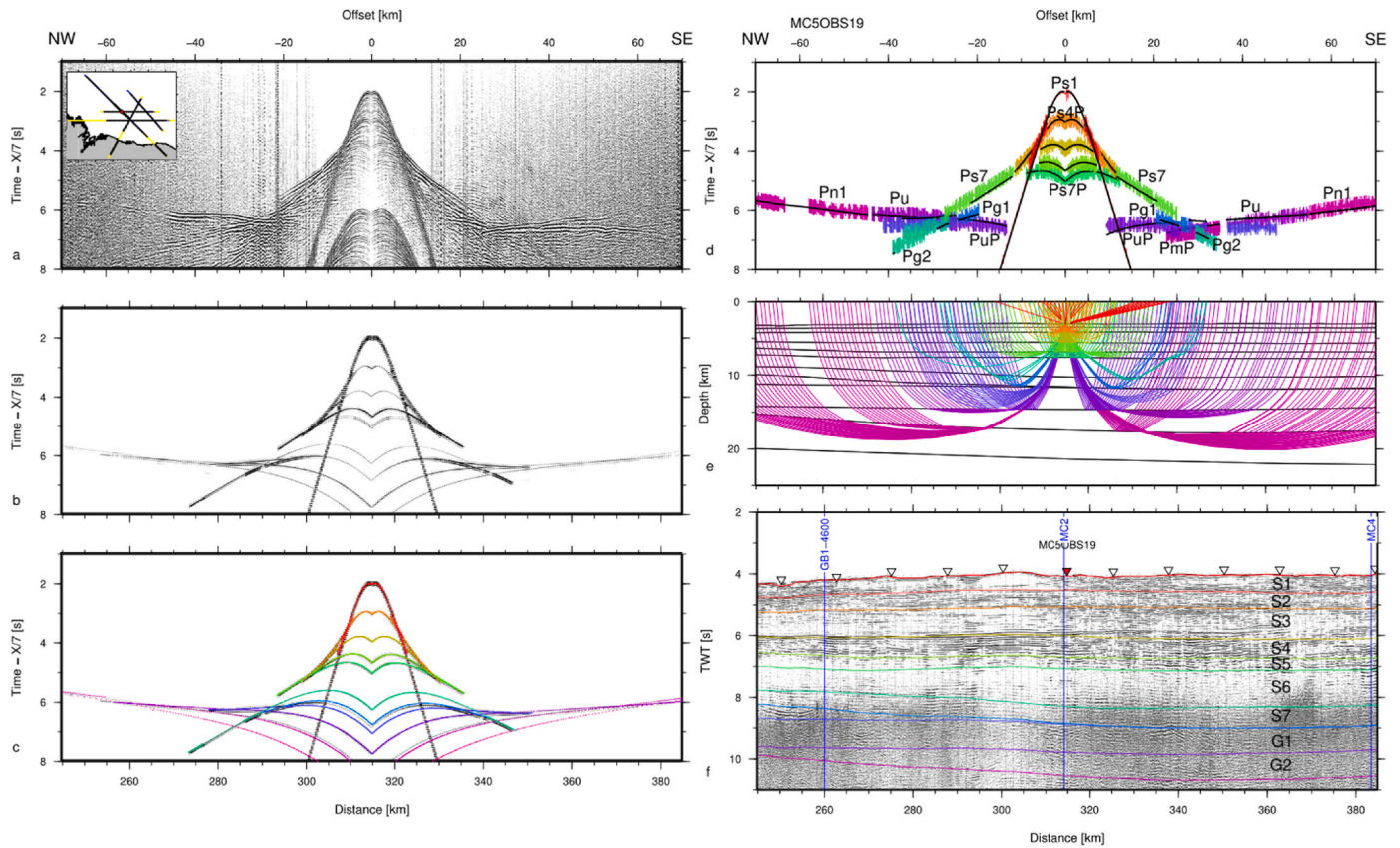


**Fig. 6.** MC5OBS19 on profile MC5 in the Basin II. a) Seismic record. b) Synthetics. c) Color coded synthetics. d) Color-coded observed travel-times overlain by predicted times in black. e) Seismic rays. f) MCS time migrated section and color-coded model interfaces. On a, b, c, and d, travel-time is reduced by a velocity of 7 km/s.

stopping criteria being a normalized  $\chi^2$  approaching to 1.

From OBS and LSS records, we digitized 103614 events and interpreted their respective phases. Travel-time uncertainty was computed from the ratio of signal energy (in a 20 ms window) to average energy in the 68 ms preceding the signal according to Zelt and Forsyth (1994). Our final velocity model is composed up to 7 sedimentary, 2 crustal, and 5 mantelic layers (Fig. 11). The model explains the travel-time and phase of 82196 events or 77% of total picks, with a global RMS travel-time residual of 0.127. Given our events individual (data driven) uncertainty, the model results in a normalized chi-squared of 1.338. In the sedimentary layers, reflected events are considerably more numerous (15476 versus 9392) and better predicted than the refracted events (Table 1). The crust along MC5 is constrained by 16760 events while the structure of the mantle is by 28439 events with rays traveling as deep as 55 km below the margin’s necking zone. The mantelic phases present the largest misfit (Pn12 and Pn13), mostly because the events travel the largest distances. MC5OBS01 on the shelf, MC5OBS07, MC5OBS15, and MC5OBS17 in the Basin II produce records at sea with the largest misfit followed by the area around the 2 volcanoes (MC5OBS38, Fig. 4); MC5LSS06, MC5LSS11, and MC5LSS14 show the poorest signal on the land records accompanied by large travel-time misfit (Table 2).

The final velocity model (Fig. 11) presents a velocity of 1.9 km/s near the sea-bottom, reaching in S5 4.5 km/s at the center and 5.25 km/s at the base of Basin II. Below in the basement layer the velocity ranges from 5 km/s to 5.9 km/s, from the NW to the SE on land on MC5 profile. The G1 base velocity is 6 km/s at the NW and 6.15 km/s at 325 km model distance where G1 pinches out. From 450 km distance to the SE limit, the G1 base velocity increases from 6.2 to 6.25 km/s. The G2 layer presents very continuous velocity across the deep-sea portion of MC5 profile: velocity increases from 6.1 to 6.25 km/s at its top and 6.9–7.1 km/s at its base from NW to SE, while 6.2 km/s at its top and 6.8 km/s at

its base are observed in the necking and on the continent. Moreover, between 260 km and 500 km model distance an up to 3 km thick high-velocity unit is imaged below G2: velocity is estimated at 7.4 km/s at its top and 7.6 km/s at its base. This layer is needed in order to fit the 2-branches Pu + Pn1 arrivals observed from MC5OBS24 to MC5OBS01. Finally, upper mantle velocity is continuous across the MC5 profile: 7.9 km/s at the Moho and 8.1 km/s at the base of this M1 mantelic layer. Three more mantelic layers are needed to fit the trains of sea-land arrivals recorded on MC5LSS01 to MC5LSS21 (Figs. 9 and 10). The estimated top and bottom velocity are 8.15–8.22 km/s in M2, 8.32–8.38 km/s in M3 and constant 8.38 km/s in M4.

### 3.1. Kernel evaluation of the model

Interface depth node spacing as well as velocity node spacing (Fig. 12a) is key to model the lateral variations of the seismic velocity with sufficient resolution, in particular where the interface geometry is well constrained in twt from the MCS data, but without introducing spurious and unwarranted complexity. Most interface and velocity nodes in our experiment produce a hit-count larger than 1000 rays (Fig. 12 b) with exception of the sedimentary and crustal layers in Basin III, as well as the deepest layer in the mantle. Since the model adopts a single velocity and velocity gradient in the upper mantle, hit-count large than 1500 is obtained on the velocity nodes as deep as 50 km. Hit-count on the interface nodes locally drops to less than 1000, most notably at the Moho below Basin III and in the necking zone. The Spread Point Function (SPF - Fig. 12 c) however indicates that lateral variations are more critical to the fitting of the interpreted data in the SPdFZ, the igneous and volcanic area and into Basin III, when compared to the sedimentary Basin II for example. As a matter of facts, larger velocity contrasts are observed in the former areas than in the latter’s, resulting

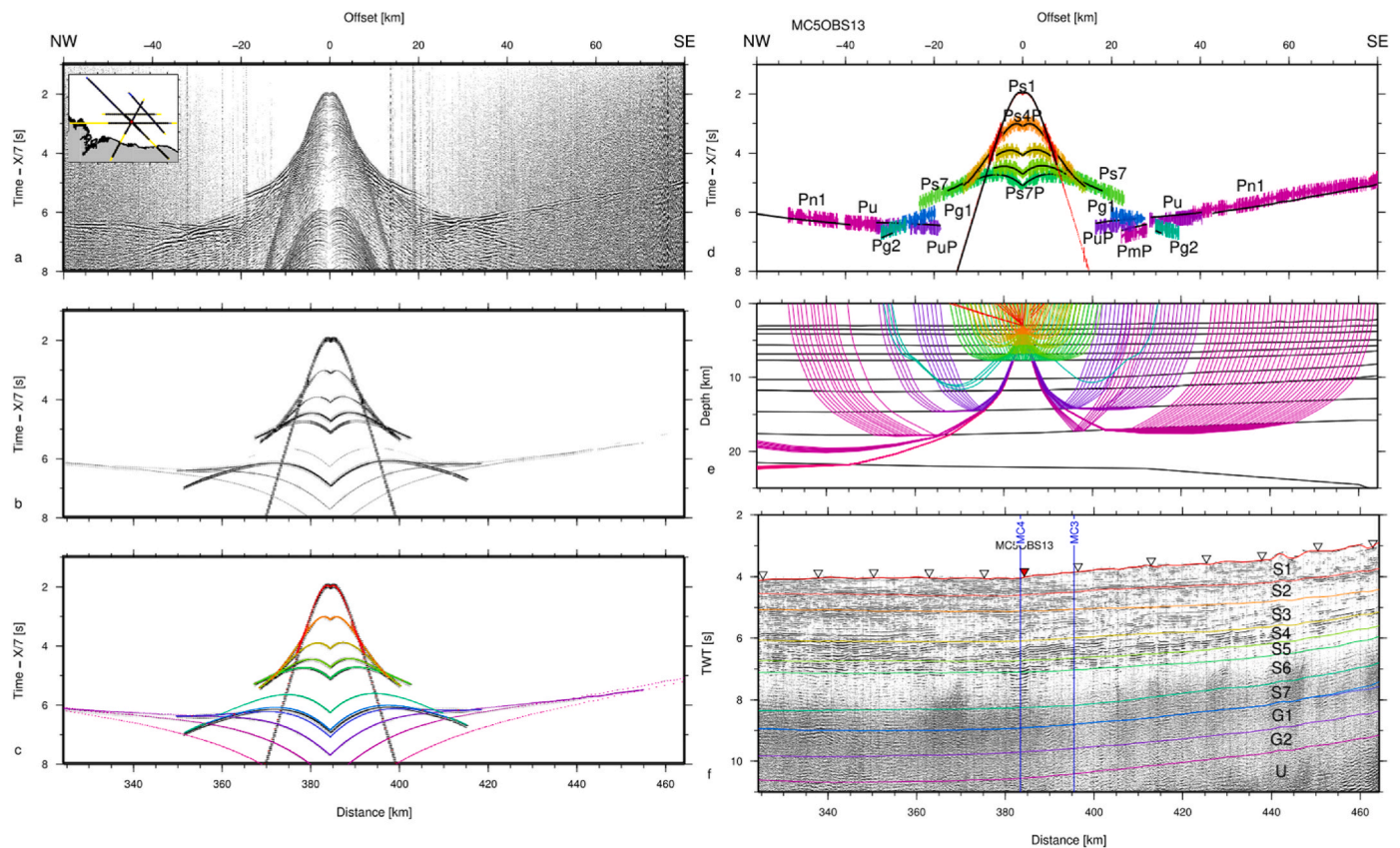


**Fig. 7.** MC5OBS13 on profile MC5 in the Basin II. a) Seismic record. b) Synthetics. c) Color coded synthetics. d) Color-coded observed travel-times overlain by predicted times in black. e) Seismic rays. f) MCS time migrated section and color-coded model interfaces. On a, b, c, and d, travel-time is reduced by a velocity of 7 km/s.

in larger travel-time variations (due to more different ray paths) for a given velocity variation in both domains, and thus a lower Spread in the inversion. Finally, the diagonal terms of the resolution matrix is a measurement of the spatial averaging of the true earth structure by a linear combination of model parameters (Zelt, 1999). Typically, resolution matrix diagonals greater than 0.5–0.7 are said to indicate reasonably well-resolved model parameters (e.g. Lutter and Nowack, 1990). The major part of the interface and velocity nodes present good resolution ( $>0.7$ ). Resolution is poorest at both extremities of the model, onland in the continental upper-crust (where rays are sub-vertical and sub-parallel), and in the deeper mantle. Also, small patches of low resolution are produced in Basin II, suggesting that the velocity variations in the basin are not fully resolved. The nodes defining the depth of the Moho in the necking zone are well resolved where the Moho plunges (from 12.75 to 14 km depth) and where it flattens in the continent (from 29 to 32.5 km depth): the Moho may have a more complex shape, but restricted by an approximately 10 km wide shadow zone (Fig. 12d).

### 3.2. Gravity modeling

A 2-D model (Fig. 13) consisting of homogeneous density blocks was constructed from the seismic velocity model: in the basement and basins, the seismic velocities are converted to densities according to Ludwig et al. (1970), resulting in densities ranging from 2200 to 2500  $\text{kg/m}^3$  in the basins, 2600–2800  $\text{kg/m}^3$  in the basement and 3100  $\text{kg/m}^3$  in the U-Unit (of Unknown composition/nature). The mantle density is set at 3200  $\text{kg/m}^3$ . The model is extended to 90 km depth and laterally by 100 km on either sides in order to avoid edge effects. Finally, the modeled free-air anomaly (Sandwell and Smith, 2009; Pavlis et al., 2012) is compared to that observed along the profile. Free-air gravity from satellite data extracted along the MC5 profile presents broad

( $>100$  km wavelength) amplitude variations of  $\pm 100$  mGal which follow the geological segmentation, the largest variations occurring at the SPdFZ and volcanoes as well as at the continental necking (Fig. 13). Due to the high altitude of the satellite, lower wave-length are not well recorded. The forward model presents the highest miss-fit of 98 mGal at the continental necking, but elsewhere fits reasonably well (within less than 25 mGal) the observed free air anomaly. On the continental shelf, the free air gravity reveals a complex 3-dimensional structure (Fig. 13) where MC5 profile cross Atlântico High, the Piauí Basin, the possible limit between Parnaíba Platform and Acaraú Basin, the southern termination of the Ceará High, and the Transbrasiliano Lineament (Sobral-Pedro II Shear Zone). Onland in the vicinity of MC5LSS06.

The load anomaly represents the pressure variation at 80 km compensation depth resulting from the lateral variations of the depth-integrated density with respect to its average along the whole profile. This anomaly therefore characterizes non-isostatic conditions and/or inaccurate velocity to density conversion. The load anomaly is generally lower than 100 Bar, but reaches 300 Bar at the crest of the volcano and 500 Bar in the necking zone.

Hence, the gravity modeling serves as an evaluation of the seismically derived model without the attempt of an arguable joint inversion.

### 3.3. MCS data pre-stack depth migration (PSDM)

Finally in order to verify the accuracy of the wide-angle velocity model, the MCS streamer data is Kirchhoff pre-stack depth migrated (MC5 PSDM profile, Fig. 14)) and residual move-out analysis is performed.

The PSDM is undertaken using the Seismic Unix package (Stockwell Jr., 1999; Cohen and Stockwell Jr., 2003), and consists in 2 steps: ray tracing and seismic data depth migration. First, the velocity model is

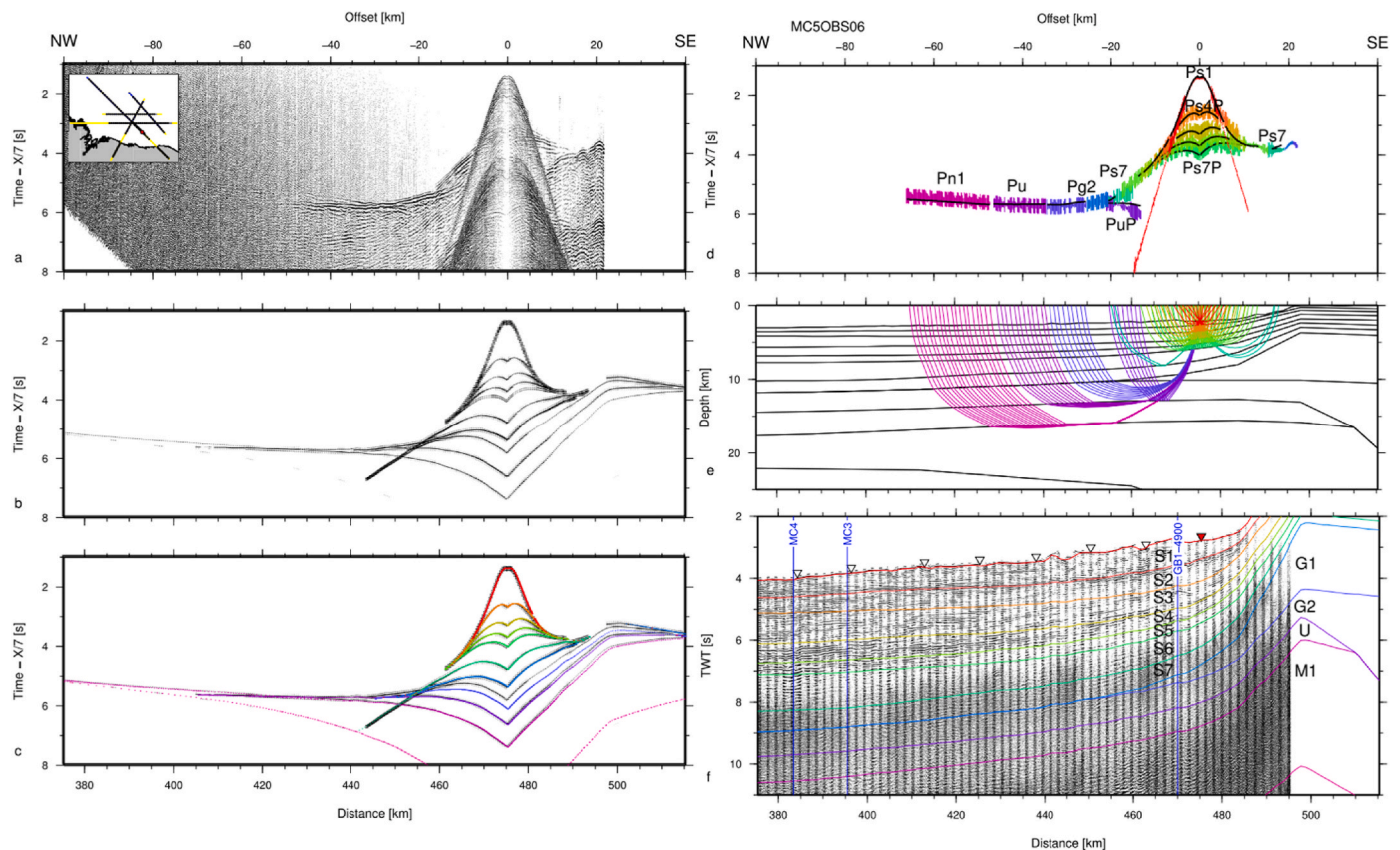


**Fig. 8.** MC5OBS06 on profile MC5 in the Basin I and continental slope. a) Seismic record. b) Synthetics. c) Color coded synthetics. d) Color-coded observed travel-times overlain by predicted times in black. e) Seismic rays. f) MCS time migrated section and color-coded model interfaces. On a, b, c, and d, travel-time is reduced by a velocity of 7 km/s.

utilized to compute travel-time tables regularly spaced at 200 m along the profile by paraxial ray tracing on a  $50 \times 24$  m spaced grid, then travel-times in shadow zones are compensated by solving the eikonal equation. The residual move-out behavior together with the seismic character from PSDM images are key elements to locate accurately major geological contacts, moreover with higher horizontal resolution when compared to OBS records. The MC5 PSDM profile (Fig. 14) shows a rather continuous seismic character up to the top of the G1 basement of our model with strong well-stratified and high-frequency reflectors. It improves particularly the imaging of the sedimentary, lava and mixed bedding, at the SPdFZ, the volcanos and Basin III. However, within the crust and at the Moho, the acquisition foot-print ( $\sim 150$  m shot spacing) severely handicaps the PSDM compared to the conventional time imaging (Fig. 2).

Moreover, we present in a companion paper (Gonçalves et al., this issue) the depth imaging resulting from the pre-stack depth migration of the OBS records by applying a reverse-time method. The contribution of the wide-angle/large offset data enhances considerably the seismic imaging along MC5 profile when compared to the MCS streamer processing, and adds support to our layer-based model.

#### 4. Discussion

In order to characterize the properties of the basins and crust and to establish the lateral segmentation along MC5 profile, 1-D velocity-depth profiles were extracted from the velocity model at 10 km interval (Fig. 15).

The sedimentary and volcano-sedimentary S1 to S7 layers.

In the shallow layers S1 to S4, the layers thickness, velocity and velocity gradient present mild variations (mostly the thickening of S3

between 200 and 480 km model distance) and rather continuous seismic character on the entire MC5MCS profile (Fig. 2). We identify as Aslanian et al. (2021) a high velocity body ( $>4$  km/s) in layer S5, 400–600 m thick that lies approximately horizontal at 6.8 km depth between 280 and 450 km model distance. The presence of considerably higher velocity in this interval is best identified by its strong refraction followed by a seismic gap on the OBS records (MC5OBS13 for example, Fig. 8) and can be traced laterally as high amplitude/low frequency continuous reflectors on the MC5PSDM (Fig. 14). Moreover, the velocity and seismic character is also preserved within layers S5 to S6 along most of the MC5 profile (Fig. 15). Near the axis of both volcanoes, the top of S5 appears to mark the highest impedance contrast. Fan-shaped reflector in S5 compose the flanks of the volcanoes on the MC5PSDM (Fig. 14), marking the last volcanic events. Further away from the volcanoes, the preserved seismic character and velocity within S5 suggest either extension of the lava as pillows or volcano-sedimentary deposit between  $-20$  and 135 km model distance, but also extending up to 475 km model distance in Basin II as seals or volcanic ashed deposit. In layer S7, while the velocity of  $\sim 4.5$  km/s at the top and 5.25 km at the base is observed all along MC5, the nature of its constituent may vary from more compacted sediments in Basin I and II, to volcano-sedimentary mixed deposit in Basin III and the SPdFZ but of contrasting seismic character of weak/discontinuous and strong/continuous reflectivity on MC5PSDM (Fig. 14) respectively. Finally, the sedimentary basin on the continental shelf, 8 km thick below MC5OBS03, appears from the wide-angle data (but without streamer data in the area) to thins rapidly toward the inland. This is also suggest by geological outcrops (the Médio Coreaú formation outcrops at MC5LSS10), gravity and aeromagnetic data (Tavares et al., 2020; de Castro et al., 2022).

The basement G1, G2 layers and U-unit.

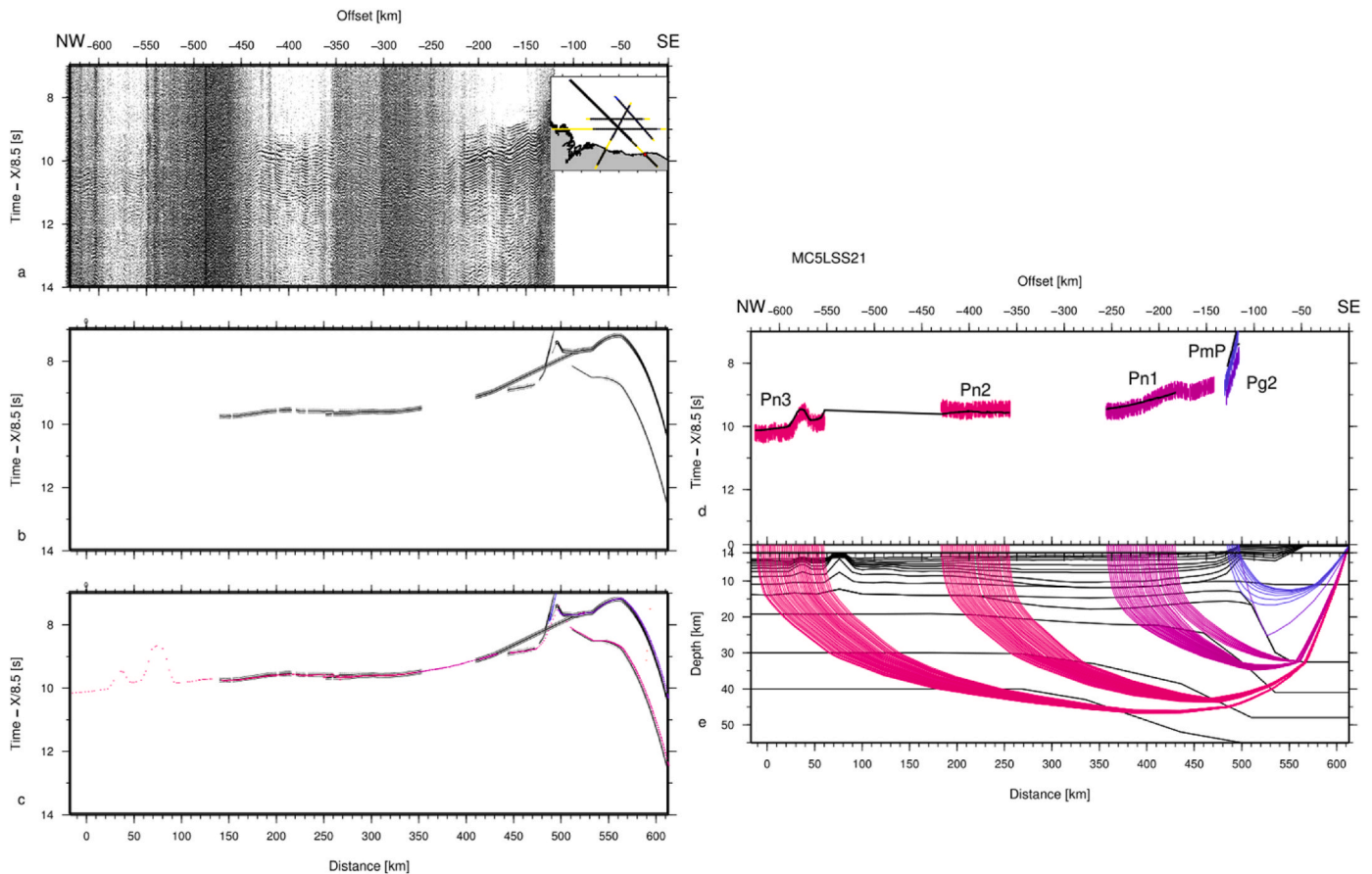


**Fig. 9.** MC5LSS21 on profile MC5 on the Parnaíba platform. a) Seismic record. b) Synthetics. c) Color coded synthetics. d) Color-coded observed travel-times overlain by predicted times in black. e) Seismic rays. On a, b, c, and d travel-time is reduced by a velocity of 8.5 km/s.

The top of the basement is not marked by a strong reflection and presents weak seismic character on MC5PSDM (Fig. 14) and is primarily identified from the OBS records and a velocity exceeding 5 km/s. Fig. 15-c presents 1-D seismic velocity profiles extracted from the top of the basement every 10 km. The basement generally shows 3 distinct velocity layers G1, G2, and U-unit and a strong velocity contrast with the upper-mantle below. At the top of G1, the velocity is 5 km/s until 150 km model distance then increases to 5.5 km/s near 325 km where the G1 layer pinches out, then exceeds 5.7 km/s below the continental slope and decreasing to 5.35 km/s at the base of the continental shelf Piauí-Camocim Basin. Associated strong reflections are observed in the SPdFZ between -20 and 25 km model distance as well in Basin III from 210 to 360 km model distance (Figs. 2 and 14). At the base of G1, the velocity is about 6 km/s in the northwestern portion of MC5 and 6.2 km/s in the southwest portion (Figs. 11 and 15). In layer G2, the top velocity increases gradually along the profile, from 6.1 km/s between -20 and 205 km-6.25 km/s at 370 km and 6.35 km/s at 470 km, then 6.3 on the continent. The basal velocity follows a similar trend from 6.9 km/s between -20 and 205 km and 7 km/s at 330 km increasing to 7.1 km/s at 470 km. Restricted to Basin II, a U-unit is imaged below at depth ranging from 13 to 18 km, and characterized by unusual/anomalous 7.4-7.6 km/s velocity significantly lower than in the upper mantle and presenting a low gradient, as observed along MC2 and MC3 profiles (Aslanian et al., 2021). The absence of G1 between 285 and 450 model distance together with the presence of the U-unit between 225 and 510 model distance, imply a non-cylindrical segmentation along the high-line margin at the edges of Basin II.

The Romanche fracture zone, Ceará margin and Borborema province of the NE Brazilian continent.

The Ceará margin is bounded by the RFZ to the north and the

Borborema province to the south. This margin is segmented by the Precambrian Tentugal and Transbrasiliano shear zones (Tavares et al., 2020). The RFZ was originally a dextral transtensional corridor (Davison et al., 2015) and was generated as a continent-continent transform fault during continental rifting (Bonatti et al., 1991). Recent studies have reported seismicity and present-day faulting along the RFZ and its splay fault onshore (Attoh et al., 2004; Kutu, 2013; Andrade et al., 2018).

A gap of 70 km separates MC5OBS01 on the continental shelf from MC5LSS21 deployed near the shoreline and shooting only extended to MC5OBS05, creating a shadow zone in the upper layers where velocity can not be determined from our data (Fig. 11). Similarly, the precise geometry of the continental margin along our transect is under determined lacking onshore reverse shots for arrivals at the land stations, since both depth of the Moho and crustal velocities in the upward traveling rays need to be inverted together. Fortunately, a deep seismic refraction experiment was carried out in the Borborema Province in November 2008 (INCT-ET/CNPq. de Lima et al., 2015). This profile resolves the seismic structure of the lithosphere along an 880 km long transect that runs 50 km SE of MC5 profile. Their results conclude that the continental crust is about 35 km thick composed of 2 layers separated at about 12 km depth, with a velocity of 5.8-6 km/s at the top and 6.2-6.3 km/s at the base of the upper crust, and 6.4-6.5 km/s at the top and 6.6-6.8 km/s at the base of the lower crust. Furthermore, receiver functions computed along the INCT-ET/CNPq profile indicates a crustal thickness of 30-36 km.

Our results are in good accordance with velocity determined at the INCT-ET/CNPq experiment. The velocity and velocity gradient and layer thickness in G1 and G2 follow remarkably well one published by Christensen and Mooney (1995) for typical thinned continental crust from 530 km to 700 km model distance. Two domains in the necking

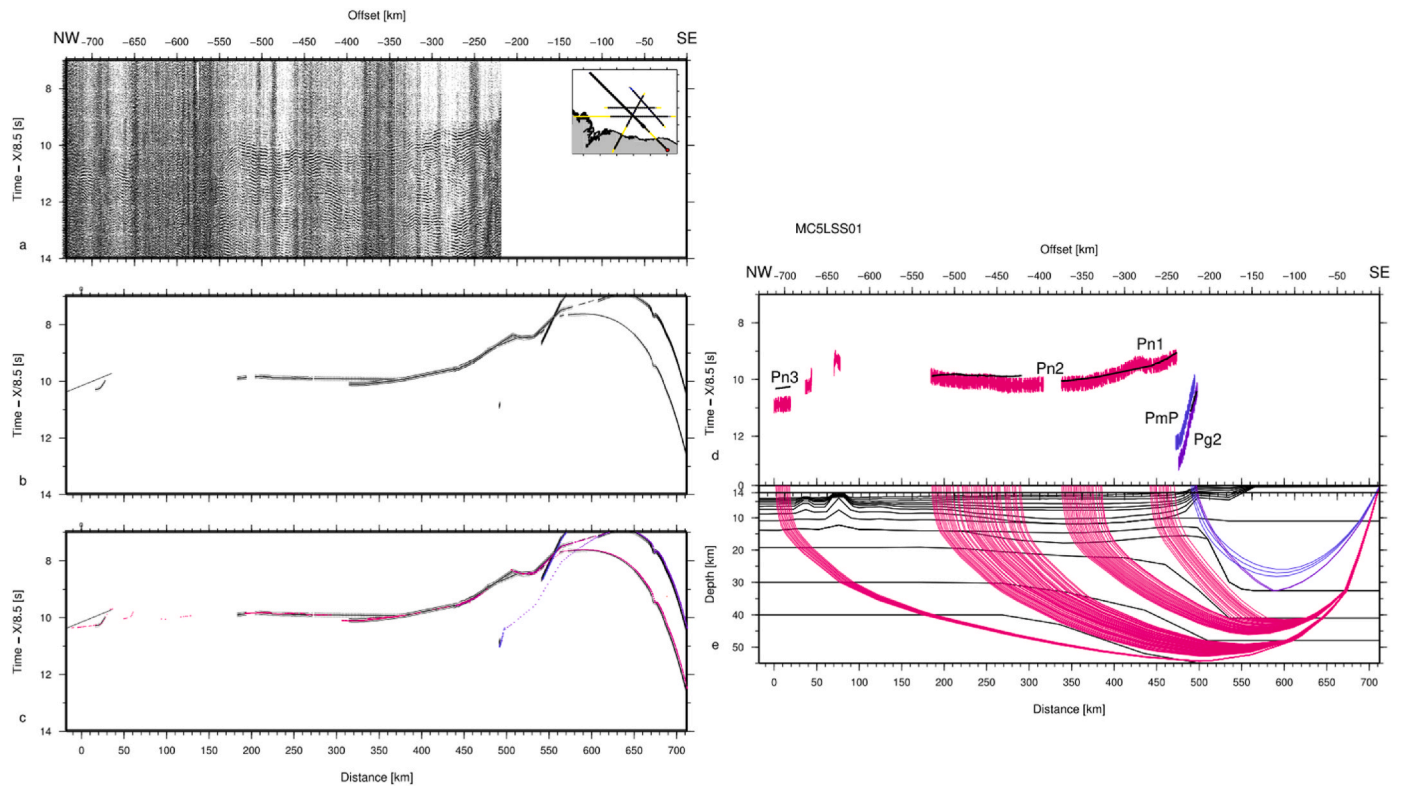


Fig. 10. MC5LSS01 on profile MC5 on the Ceará basin. a) Seismic record. b) Synthetics. c) Color coded synthetics. d) Color-coded observed travel-times overlain by predicted times in black. e) Seismic rays. On a, b, c, and d travel-time is reduced by a velocity of 8.5 km/s.

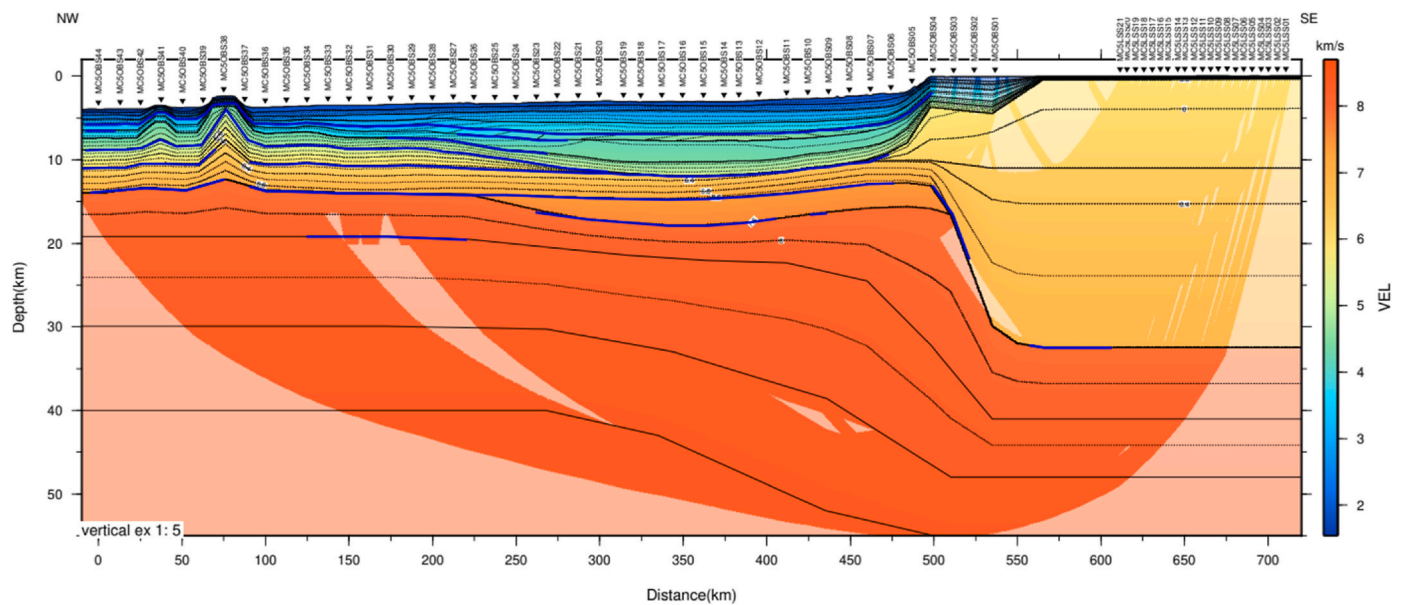


Fig. 11. Acoustic velocity model of MC5 profile shaded by illumination. Layers are indicated by thick black lines and reflective interfaces are marked by blue lines. Iso-velocity contours are indicated by thin dashed lines. The location of the OBS/LSS recording instruments are marked by black triangles.

zone can be distinguished: between 560 km and 520 km model distance where both upper and lower continental crust thin to appreciatively half their thickness without a significant change in either velocity or velocity gradient (Fig. 15), and between 500 km and 460 km model distance where the Moho lies flat near 14 km depth and the crust seaward thins from 12 km to 5 km thickness. In the later zone, the thinning of the lower continental crust does hardly affect its velocity and velocity gradient.

The crustal nature of G1, G2 layers and U-unit.

Within the frame of the MAGIC survey, the structural segmentation of the Parã-Maranhão-Barreirinhas passive margin in the Equatorial Atlantic was investigated by Aslanian et al. (2021) along the MC2 and MC3 (and to some extent MC4) wide-angle profiles (Fig. 1) oriented ~ E-W close to the direction of opening. From their analysis, these authors document from west to east a 33 km thick unthinned continental crust below the Sao Luís Craton, followed by a 60 km wide necking domain below the Ilhade Santana Platform where the continental thickness

**Table 1**

Reflected or refracted phase name, number of explained events, root mean-square travel-time residual, and normalized chi-squared value.

phase	npts	Trms	Chi <sup>2</sup>
Ps2	3	671	0.054
Ps3P	4	2942	0.030
Ps3	5	1742	0.065
Ps4P	6	2893	0.026
Ps4	7	1528	0.048
Ps5P	8	3064	0.043
Ps5	9	2394	0.079
Ps6P	10	5475	0.058
Ps6	11	660	0.115
Ps7P	12	363	0.086
Ps7	13	1670	0.107
Pg1P	14	249	0.143
Pg1	15	2831	0.114
Pg2P	16	1447	0.103
Pg2	17	4739	0.171
PmP	18	4146	0.130
Pn1	19	3097	0.146
Pn2P	20	817	0.141
Pn2	21	17386	0.151
Pn3P	22	706	0.170
Pn3	23	2726	0.107
Pn4	25	6425	0.255
Pn5	3	671	0.054

decreases from about 35 km to 10 km. Ocean ward, an intermediate Basin II domain presents a 5–7 km thick sedimentary sequence, with a volcanic-sedimentary interbedded layer characterized by 5 km/s high seismic velocity. According to this study, Basin II would lie on a substratum made of exhumed lower continental crust, overlying a layer characterized by anomalous 7.4–7.6 km/s acoustic velocity (AVL unit), interpreted as possible evidence of intrusions of mantle-derived melts into the deeper exhumed lower continental crust. [Tavares et al. \(2020\)](#) propose that the Barreirinhas basement is composed of hyper-extended continental crust, based on a set of ~NS seismic profiles and gravity data inversions extending from the RFZ into the deep basin. According to [de Castro et al. \(2022\)](#), this continental basement extends eastward up to the NE-SW-oriented Tentugal shear zone, suggesting structural inheritance and crustal segmentation of the margin controlled by Precambrian shear zones. Eastwards and parallel to the hinge line, a NW-SE oriented volcano alignment marks the disappearance of the AVL ([Aslanian et al., 2021](#)). These continental basement layers would delimit the ocean-ward extend (~150 km wide) of the main thinning phase of the north-eastern Brazilian margin within this divergent segment during the west-Gondwana breakup and initiation of the equatorial Atlantic formation.

The transition to oceanic crust is more complex than expected, with the presence of an about 60 km-wide band of proto-oceanic crust ([Fig. 1](#)), before a “more typical” but still thin oceanic crust eastward ([Aslanian et al., 2021](#); [Moulin et al., 2021](#)). This proto-oceanic crust presents, in its upper part, seismic velocity higher than “normal” oceanic crust but in continuity with the velocity described in the intermediate domain. In this proto-oceanic domain, [Moulin et al. \(2021\)](#) describes, from the analysis of MC1 profile, parallel to our MC5 and also spanning between the two main SPdFZ and RFZ, ~5.5 km of sedimentary deposits overlying a 5 km-thick crystalline basement presenting two layers characterized by high acoustic velocity and a very sharp Moho at the base. [Fig. 16](#) provides a schematic summary of the structural interpretation of the 5 MAGIC survey wide-angle profiles.

While the central part of MC5 profile (MC5OBS11 to MC5OBS25) spans within the intermediate domain of Basin II identified on MC2 and MC3 profiles ([Fig. 1](#)), this profile expands ~225 km NE-ward into the volcano alignment and the SPdFZ, and thus provides the opportunity to examine the cylindricity of the divergent Par -Maranh o margin and the nature of the crust in the transform segment bounding the Foz do Amazonas divergent segment to the north. According to the 1D profiles

**Table 2**

Instrument name, distance along model, direction code (–1 for rays traveling southward and 1 traveling northward), number of explained events, root mean-square travel-time residual, and normalized chi-squared value.

Instrument	X_Shot	dir	Npts	RMS	Chi2
MC5OBS44	0.001	–1	436	0.058	0.449
	0.001	1	715	0.061	0.339
MC5OBS42	25.084	–1	632	0.072	0.517
	25.084	1	772	0.177	2.829
MC5OBS41	37.495	–1	462	0.120	1.745
	37.495	1	433	0.117	1.235
MC5OBS40	50.454	–1	564	0.107	2.897
	50.454	1	508	0.135	2.226
MC5OBS39	62.634	–1	420	0.098	1.716
	62.634	1	732	0.233	3.153
MC5OBS38	75.143	–1	334	0.169	5.933
	75.143	1	429	0.099	4.406
MC5OBS37	87.635	–1	314	0.218	2.056
	87.635	1	390	0.067	0.337
MC5OBS36	100.165	–1	636	0.091	0.858
	100.165	1	808	0.064	0.948
MC5OBS35	112.726	–1	588	0.126	1.150
	112.726	1	978	0.124	1.594
MC5OBS34	125.116	–1	668	0.231	4.356
	125.116	1	894	0.067	0.698
MC5OBS33	137.697	–1	820	0.062	0.512
	137.697	1	994	0.125	1.486
MC5OBS32	150.217	–1	726	0.074	0.965
	150.217	1	789	0.120	2.339
MC5OBS31	162.699	–1	1168	0.067	0.494
	162.699	1	898	0.090	0.982
MC5OBS30	175.210	–1	1012	0.081	0.780
	175.210	1	1386	0.120	3.128
MC5OBS29	187.741	–1	745	0.133	2.912
	187.741	1	1110	0.133	2.538
MC5OBS28	200.244	–1	847	0.114	0.932
	200.244	1	831	0.096	1.637
MC5OBS27	212.821	–1	823	0.111	1.383
	212.821	1	971	0.123	2.323
MC5OBS26	225.228	–1	1047	0.139	3.088
	225.228	1	840	0.078	0.745
MC5OBS25	237.821	–1	930	0.168	2.240
	237.821	1	816	0.089	1.576
MC5OBS24	250.278	–1	958	0.124	1.457
	250.278	1	1289	0.127	12.419
MC5OBS23	262.792	–1	702	0.158	1.231
	262.792	1	486	0.101	1.890
MC5OBS22	275.161	–1	730	0.061	0.515
	275.161	1	794	0.086	1.049
MC5OBS21	287.770	–1	935	0.078	0.949
	287.770	1	935	0.124	1.728
MC5OBS20	300.343	–1	569	0.155	2.383
	300.343	1	846	0.115	1.741
MC5OBS19	314.833	–1	882	0.092	1.608
	314.833	1	984	0.108	1.250
MC5OBS18	325.345	–1	814	0.093	2.597
	325.345	1	535	0.108	1.958
MC5OBS17	337.769	–1	619	0.079	0.764
	337.769	1	537	0.110	4.831
MC5OBS16	350.313	–1	670	0.139	1.300
	350.313	1	618	0.128	1.226
MC5OBS15	362.814	–1	954	0.140	2.016
	362.814	1	609	0.124	1.146
MC5OBS14	375.270	–1	662	0.144	2.279
	375.270	1	634	0.110	0.957
MC5OBS13	384.294	–1	753	0.064	2.284
	384.294	1	850	0.118	1.164
MC5OBS12	396.345	–1	696	0.099	1.206
	396.345	1	625	0.068	0.471
MC5OBS11	412.857	–1	659	0.096	0.636
	412.857	1	581	0.105	1.103
MC5OBS10	425.339	–1	568	0.063	0.801
	425.339	1	464	0.065	0.828
MC5OBS09	437.885	–1	648	0.069	0.439
	437.885	1	491	0.076	0.669
MC5OBS08	450.411	–1	628	0.116	0.928
	450.411	1	438	0.073	0.491

(continued on next page)

Table 2 (continued)

Instrument	X_Shot	dir	Npts	RMS	Chi2
MC5OBS07	462.892	-1	527	0.057	0.291
	462.892	1	283	0.069	1.615
MC5OBS06	475.329	-1	561	0.079	0.900
	475.329	1	264	0.092	1.617
MC5OBS05	487.863	-1	437	0.141	1.095
	487.863	1	109	0.052	0.214
MC5OBS04	500.450	-1	564	0.197	3.122
MC5OBS03	512.862	-1	371	0.049	0.201
MC5OBS02	525.356	-1	394	0.077	0.514
MC5OBS01	537.979	-1	266	0.102	11.104
MC5LSS21	612.911	-1	884	0.149	1.198
MC5LSS20	616.865	-1	708	0.125	0.672
MC5LSS19	622.006	-1	813	0.228	3.199
MC5LSS18	627.023	-1	944	0.222	1.932
MC5LSS17	632.149	-1	579	0.106	0.473
MC5LSS16	637.061	-1	336	0.127	0.636
MC5LSS15	641.495	-1	504	0.109	0.378
MC5LSS14	647.489	-1	499	0.114	1.859
MC5LSS13	651.569	-1	704	0.136	0.829
MC5LSS12	657.184	-1	387	0.086	0.411
MC5LSS11	662.320	-1	636	0.495	12.951
MC5LSS10	667.131	-1	662	0.130	0.604
MC5LSS09	671.815	-1	399	0.175	1.263
MC5LSS08	677.122	-1	195	0.138	1.654
MC5LSS07	682.138	-1	163	0.075	0.420
MC5LSS06	687.032	-1	872	0.345	4.804
MC5LSS05	692.156	-1	942	0.241	2.336
MC5LSS04	697.321	-1	142	0.100	0.360
MC5LSS03	701.846	-1	155	0.162	1.132
MC5LSS02	707.123	-1	283	0.257	4.009
MC5LSS01	712.147	-1	759	0.197	1.525

(Fig. 15), the U-unit observed on MC5 can be interpreted as the AVL described on MC2 and MC3. Then, the total crustal thickness in the deep-sea portion of MC5 is up to 5.5 km underneath most of Basin II and decreases to 5 km in Basin III and SPdFZ. The lateral trend of the 1-D velocity in the basement presents a global decrease of  $\sim 1$  km/s at the transition from Basin II to III, where the upper-crustal G1 layer reappears and the U-Unit thins out. From the velocity alone, the determination of the crustal nature in Basin III and SPdFZ is ambiguous: the 1-D profile fall within the compilation of Atlantic oceanic crust by White et al. (1992), but magmatic events overprinted the original crustal composition. Three events were identified in the area (Tamara et al., 2020): "A Late Albian? Magmatic event in the Barreirinhas segment, A Turonian? To Campanian? Event that formed the volcanic chain in the Amazon segment that extends into the SPdFZ and Pará-Maranhão transform segment, and a Maastrichtian? Event with localized magmatism along the southern SPdFZ."

Furthermore Tamara et al. (2020) analyses the crustal structure underlying the central equatorial margins, from their continental slope to the abyssal plain based on 27 industrial seismic profiles located in an area  $\sim 600$  km along the margin from the northern part of Barreirinhas segment to the southern part of Amazon segment that comprises MC5's Basin III and SPdFZ. Part of their data set was previously published by Krueger et al. (2012) and Zalan (2015). These authors interpret the crust the area south of the SPdFZ as hyper-extended continental crust, thus also in this study's Basin III. This is in favor of a relatively cylindrical segmentation of the Barreirinhas margin parallel to the hing line. In the SPdFZ, i.e. the in the Pará-Maranhão transform segment the authors interpret exhumed and serpentinized continental mantle to the west of

MC5 and oceanic crust to the east, our profile being locate at the limit. Thus a 3rd interpretation for the nature of the basement in the SPdFZ must be considered. Finally, these authors point out that transition from exhumed mantle to oceanic crust may be similar to the hybrid transitional crust described Gillard et al. (2017) in the conjugate Ivory Coast margin. This observation raise the question of the symmetry of the Para-Maranhão-Barreirinhas and the Deep Ivory Basin-Ghana conjugate passive margins system.

As a matter of facts, Antobreh et al. (2009) outline the deep structure of the African Ghana margin using a series of 2D gravity modeled transects constrained by MCS and published wide-angle data (e.g. Edwards et al., 1997; Sage et al., 1997). The margin is divided into two distinct segments: the ENE–WSW trending sheared margin of the Cote d'Ivoire-Ghana Ridge and the NE–SW trending rift-influenced sheared margin of the Ghana Platform (e.g. Kuszniir et al., 2018; Scarselli et al., 2020; Gonçalves et al.). The deep Ivorian Basin originated as a major pull-apart associated to crustal thinning of the basin. Finally, Antobreh et al. (2009) localize the transition from continental to oceanic crust (OCB) in this area of western-equatorial Africa.

The palinspastic reconstruction of the Pará-Maranhão/Barreirinhas-Ghana-Ivory Coast rifting of the Equatorial Atlantic Ocean proposed by Moulin et al. (2021) together with the results of Aslanian et al. (2021) can therefor be complemented by the founding of this study. Thus, Fig. 17 presents a schematic evolution of the Central Equatorial Ocean along 4 stages during rifting and oceanic spreading phases, extrapolated from the fit of Moulin et al. (2010) at 112 Ma and the intermediate pole at C34 of Campan (1995) considering a constant spreading rate. Furthermore, our reconstruction initially assumes both relative symmetrical and cylindrical rifting of the 3 divergent segments of the Central Equatorial Atlantic. Small circles fit the fracture zones (nSPFZ, sSPFZ, RFZ and CFZ in Fig. 17) during this period. The COBs of Tamara et al. (2020), Tavares et al. (2020) and Aslanian et al. (2021) on the South American side and of Antobreh et al. (2009) on the African side delimit the domains of continental hyper-extension/exhumation, and inset of "mid"-oceanic crust accretion (Fig. 17c near 99 Ma). The location of this onset within the SPdFZ is matter of debate. The relatively small width of the SPdFZ in the Pará-Maranhão transform segment favors an accretion center aligned with either the Amazone or Barreirinhas segments. The observed COB of Tamara et al. (2020), together with the present-day NE-SW oriented continental coast-lines that spur a favorable mechanical week line extending from the RFZ to the nSPFZ. In this scenario, the entire African continental hyper-extended/exhumation domain of the Pará-Maranhão transfer margin would have been trapped with the Brazilian one, and would explain our findings at the NW end of our MC5 survey. This hypothesis is confirmed by the present-day  $\sim 500$  km in length asymmetry of the mid-oceanic ridge at the nSPFZ between its South-American and African sides (Fig. 17d).

## 5. Conclusions

Our MC5 wide-angle profile supports the presence along the Barreirinhas divergent margin of a  $\sim 150$  km wide basin (in the  $\sim$ E-W direction) floored by exhumed lower continental crust, 5–5.5 km thick and cylindrical (parallel to the hing-line), partly altered by an upper-mantle contribution to the base of Basin II basement and post breakup magmatism in Basin III. Basin II reaches 7 km in thickness and interleaved by a  $\sim 500$  thick high velocity ( $\geq 5$  km/s) layer that can be correlated to the

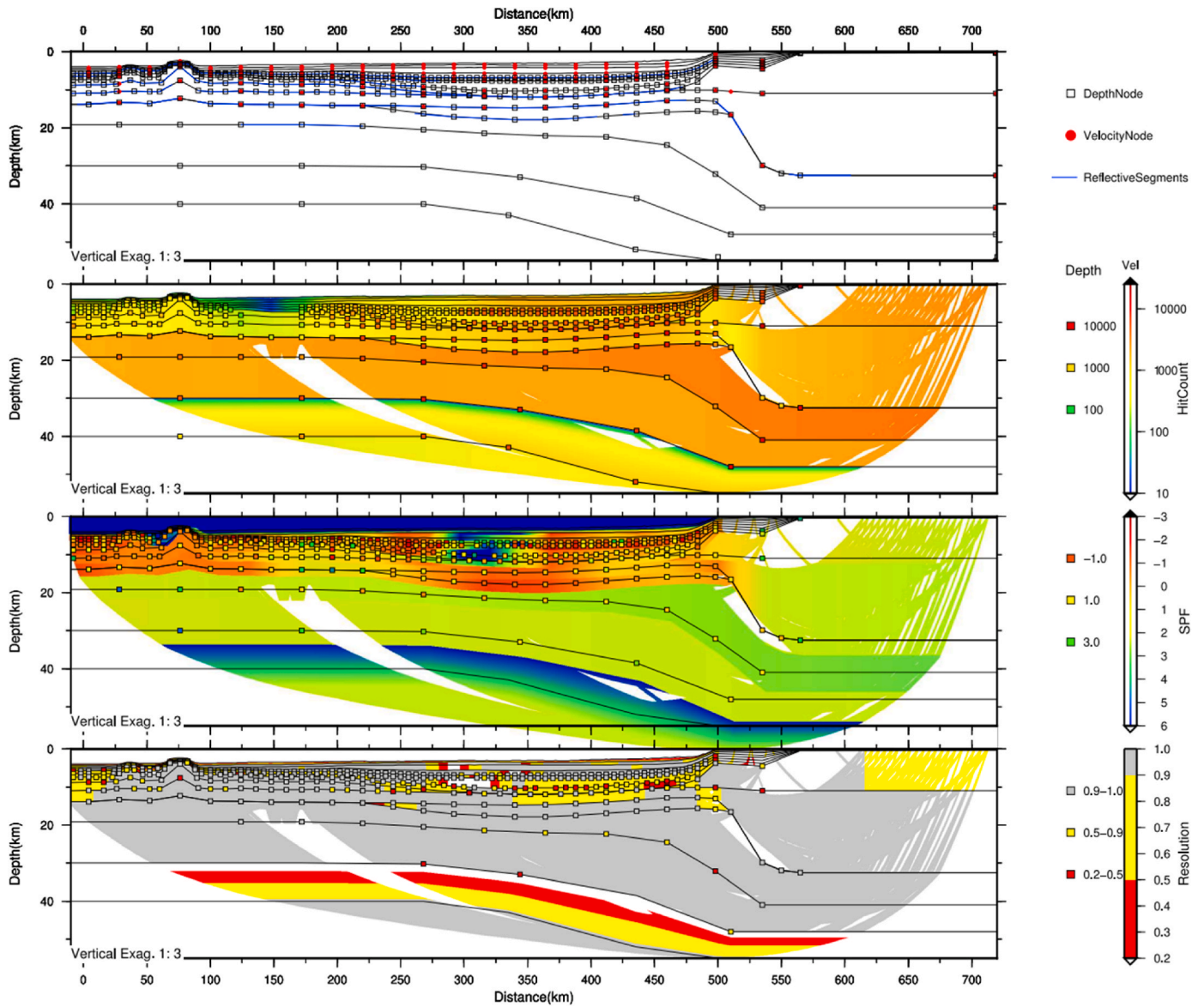


**Fig. 12.** a) Distribution of interface depth nodes and top and bottom velocity nodes of the final P-wave interval velocity model along MC5 wide-angle profile. Interfaces where reflections have been observed on OBS data are highlighted in yellow. b) Hitcount of rays traced in the model during the inversion. Depth interface nodes are plotted with squares scaled to the hitcount though the node. c) Spread-Point Function (SPF) in the model. Depth interface nodes are plotted with squares scaled to the SPF at the node. d) Resolution in the model. Depth interface nodes are plotted with squares scaled to the resolution at the node.

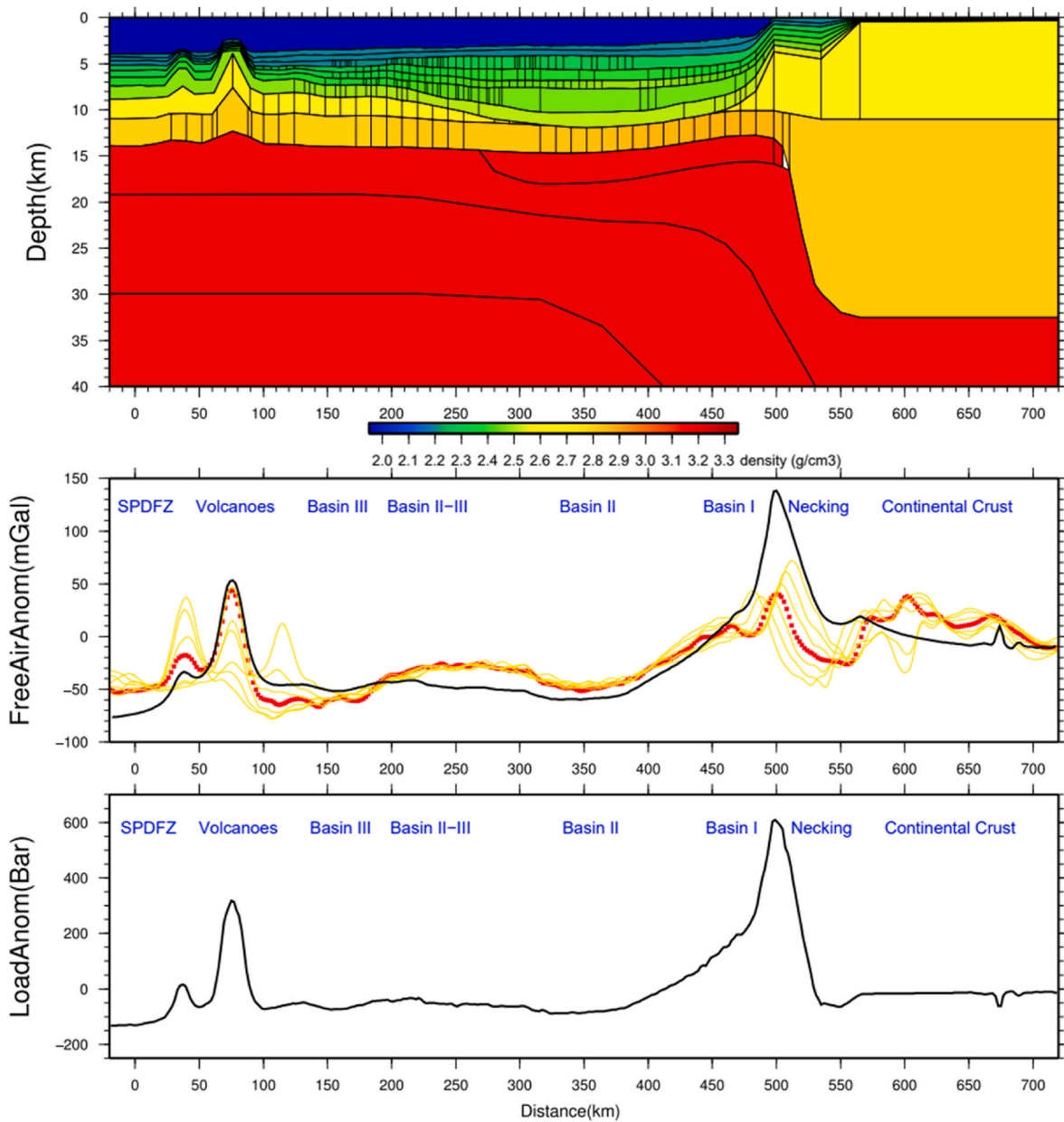


Fig. 13. Gravity model for MC5 profile overlain by interfaces from wide-angle modeling. a) Density model up to a depth of 40 km. b) Free-air gravity anomaly observed (Pavlis et al., 2012) along the MC5 profile (red dotted) and at 5, 10, and 15 km on either sides (yellow lines) and calculated (black line). c) Load anomaly.

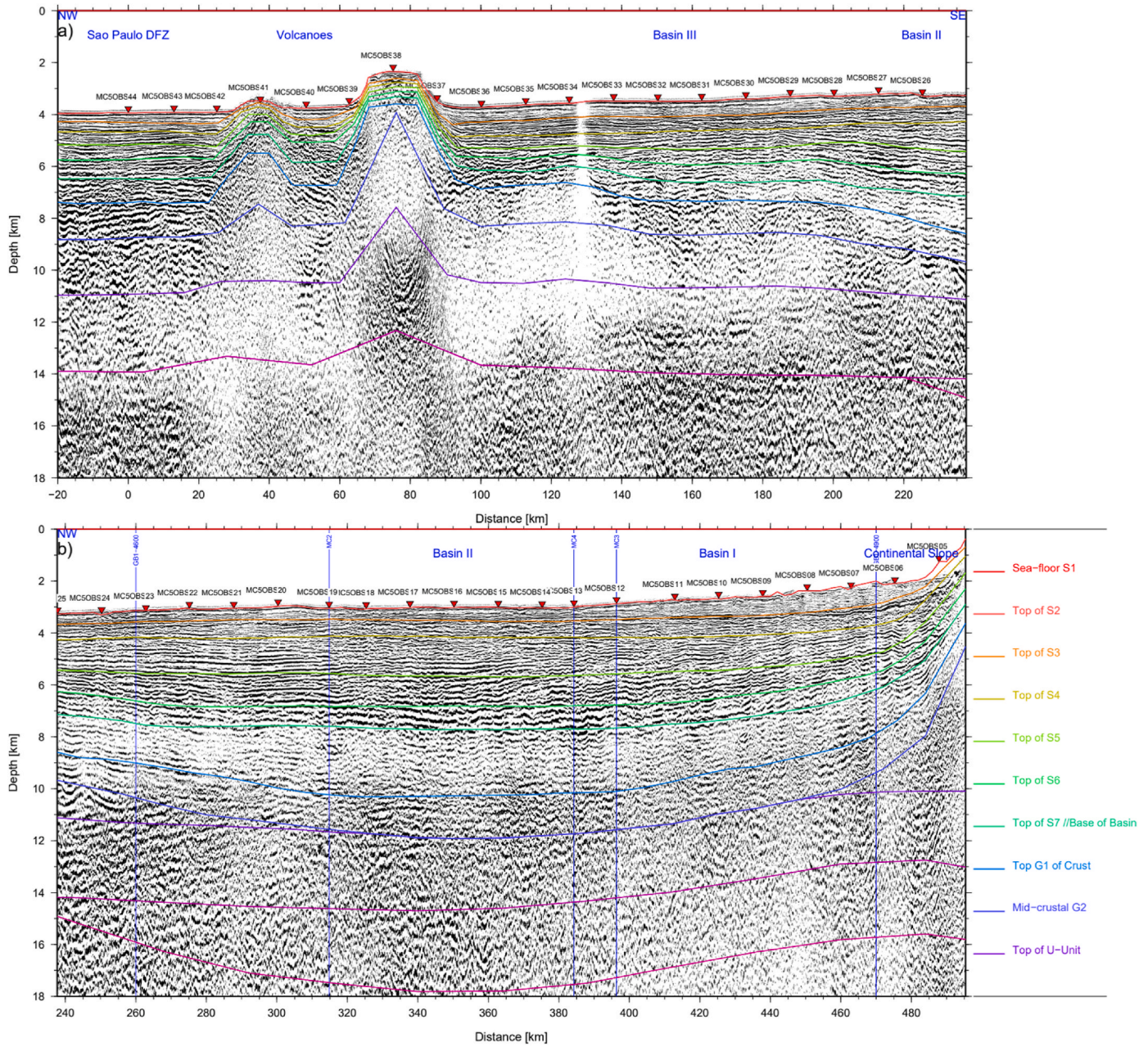
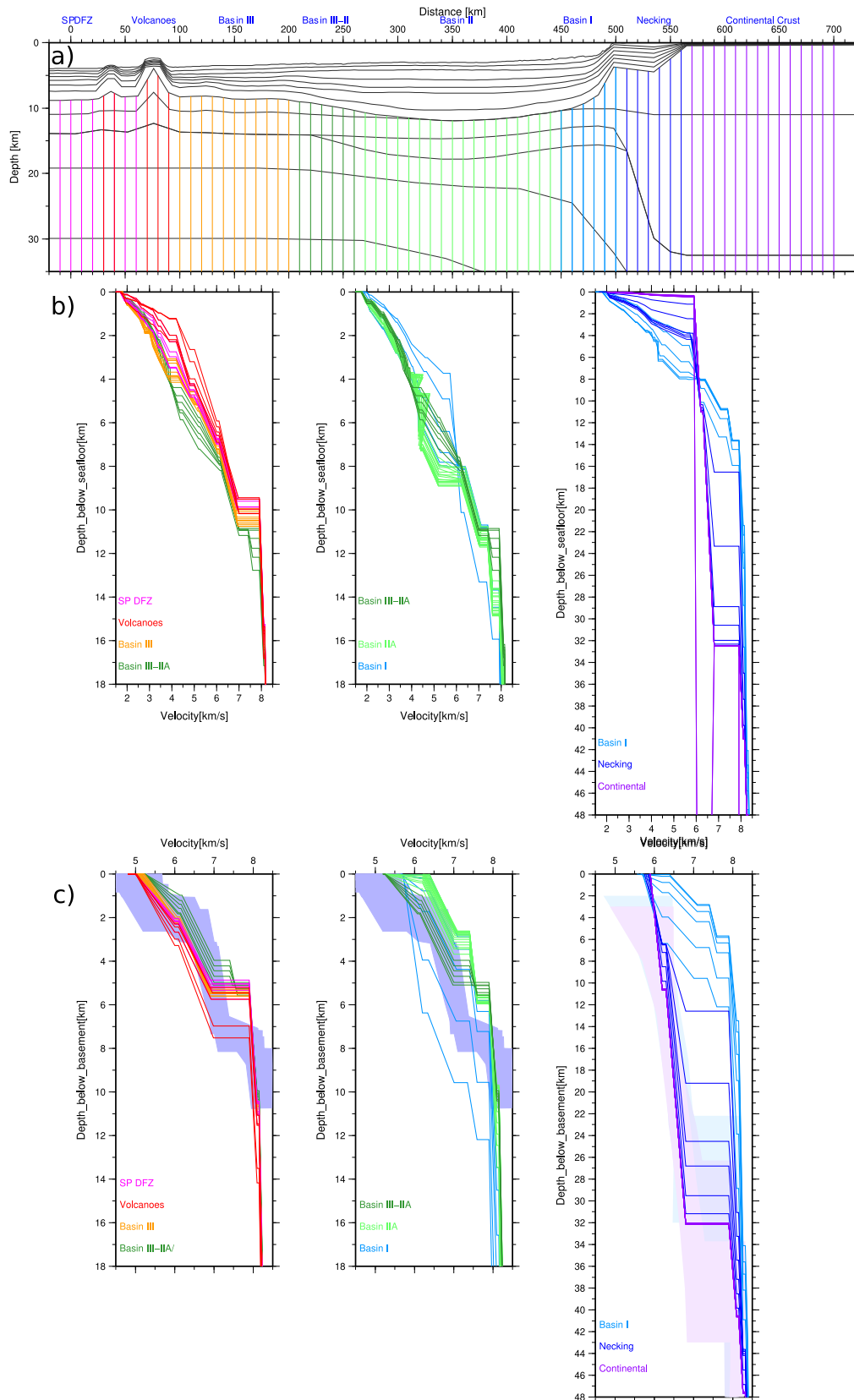
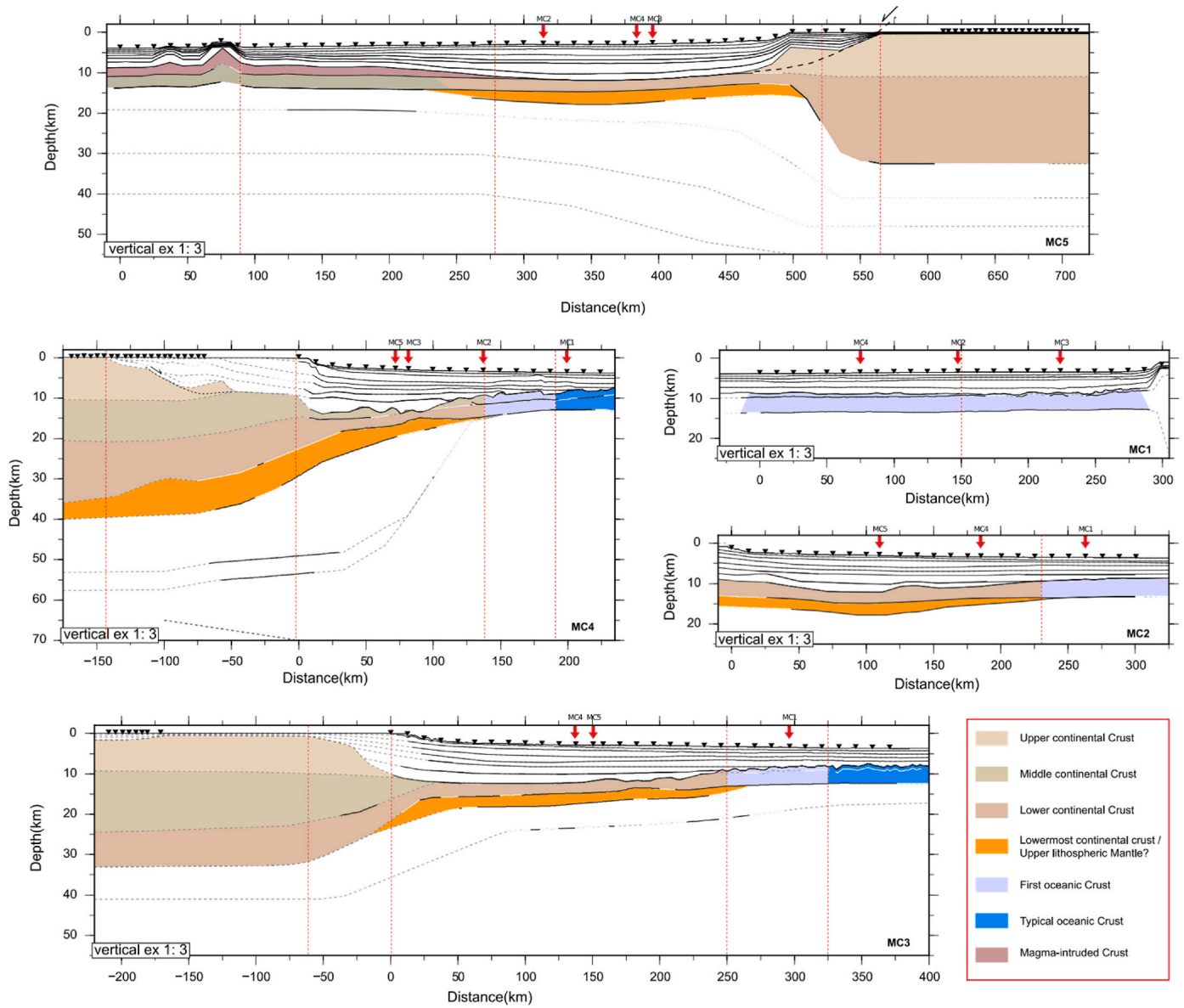


Fig. 14. Pre-stack depth migrated record section of MCS data along MC5 profile. a) Western part across the SPdFZ and Basin III. b) Eastern part across Basins II and I. Model's interfaces are represented with continuous lines. The intersections with the MAGIC and the ION GXT dataset are indicated by vertical blue lines. Vertical exaggeration is 1:5.



**Fig. 15.** a) Distribution of 1-D velocity profiles extracted from the final P-wave interval velocity model and color coded according to segmentation along the MC5 profile. b) P-wave interval velocity as a function of depth below seafloor. c) P-wave interval velocity as a function of depth below basement. From model distance 10 to 260 km (left), 210–500 km (center), and 460–700 km (right). The blue area represents the velocity range for oceanic crust compiled by White et al. (1992). The light blue, gray and pink area represents those compiled by Christensen and Mooney (1995) for extended continental crust, rifted continental crust, and shields/-platforms, respectively.



**Fig. 16.** Schematic interpretation of the crustal nature along the 5 wide-angle profiles of the MAGIC survey. MC1 is detailed in [Moulin et al. \(2021\)](#), MC2 and 3 in [Aslanian et al. \(2021\)](#), MC5, in this study and MC4 is still unpublished.

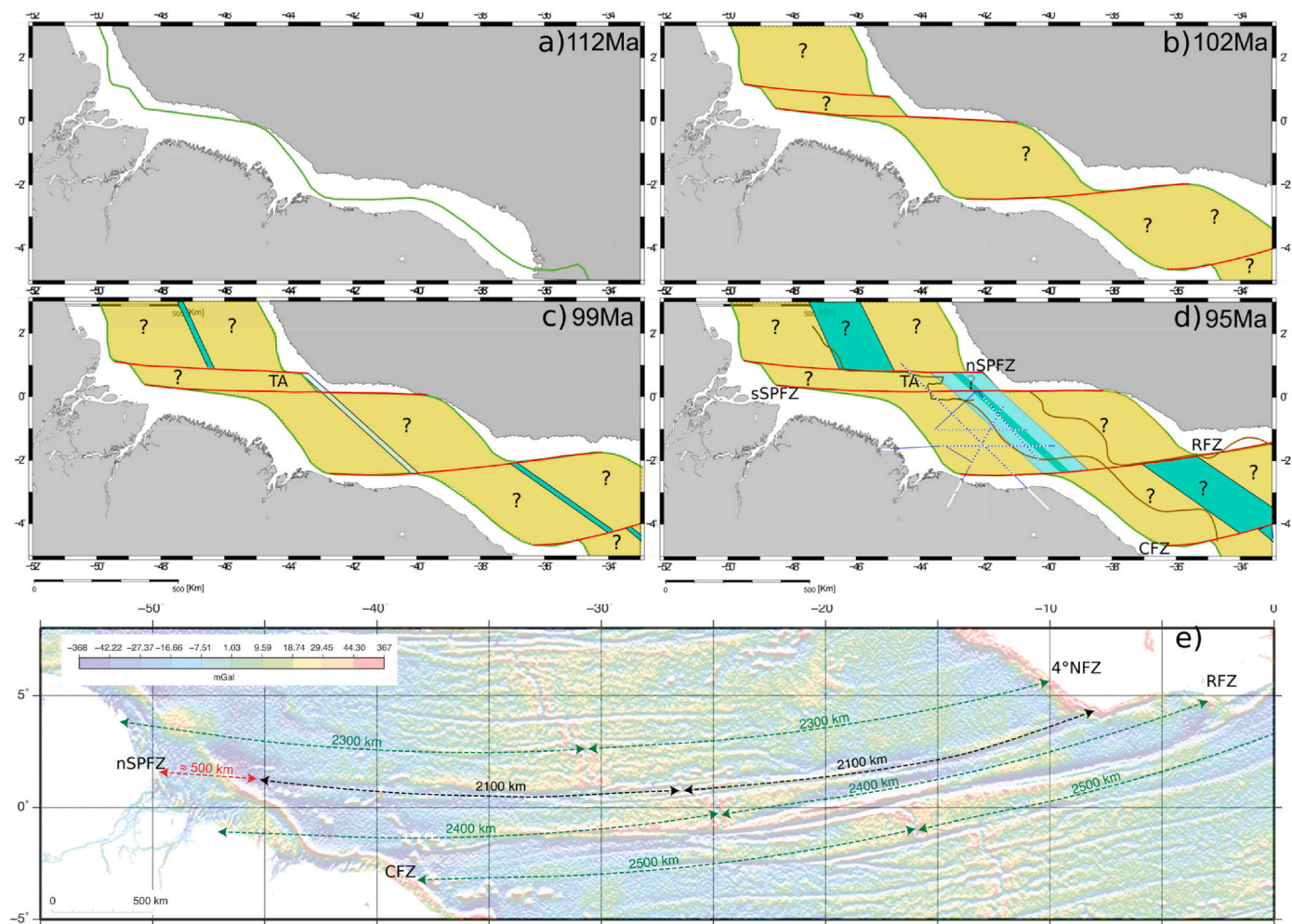


**Fig. 17.** Schematic kinematic evolution of the central Equatorial opening at: a) 112, b) 102, c) 99 and d) 95 Ma. The south American plate is fixed. The beige areas represent basins floored by hyper-extended continental crust/exhumed lower continental crust. The blue areas delineate oceanic crust, and in light blue the proto-oceanic crust proposed by the MAGIC survey analysis. Question marks characterize areas not constrained by the MAGIC survey. On d) Dark brown lines mark the south-America COB by Tamara et al. (2020), brown lines of Tavares et al. (2020) and as light-blue area from Aslanian et al. (2021), while brown lines mark the western-African COB of Antobreh et al. (2009). e) Present-day free-air gravimetric map of the central Atlantic Equatorial Ocean and length of the main fracture zones.

last magmatic events centered in Basin III volcanos as imaged by the MC5PSDM. These basins are bounded to the south by the RFZ and the strike-slip Ceará margin, characterized by a narrow  $\sim 50$  km wide necking zone in the Parnaíba Platform and associated Piauí-Camocim and Ceará Basins. Onshore in the Médio Coreáú and Ceará Central thrust belt, the un-thinned continental crust is  $\sim 32$  km thick and presents 2 distinct layers. These basins are bounded to the north by the SPdFZ: According to our wide-angle data and palinspastic reconstruction of the Pará-Maranhão/Barreirinhas-Ghana-Ivory Coast transform margin, its basement appears to be composed of a trapped piece of African exhumed lower continental crust.

#### Author contributions

The MAGIC Project was imagined by D. Aslanian and led by D. Aslanian, M. Moulin from Ifremer and A. Viana, J. Cupertino from Petrobras. The Onshore part of the project was managed by N. Dias from ISEL (Lisbon), R. Fuck and J. Soares from University of Brasília. Modeling of the MAGIC profiles was done by M. Moulin, F. Gallais, A. Afilhado and P. Schnürle. Processing of the seismic reflection data was done by P. Schnürle. The MAGIC Team is composed by: A. Baltzer<sup>6</sup>, M. Rabineau<sup>7</sup>, Z. Mokkedem<sup>7</sup>, M. Benabdelhouahed<sup>7</sup>, M. Evain<sup>1</sup>, A. Lour-eiro<sup>3</sup>, D. Alves<sup>3</sup>, F. Klingelhoefer<sup>1</sup>, R. Apprioual<sup>1</sup>, J. Crozon<sup>1</sup>, P.

Fernagu<sup>1</sup>, D. Le Piver<sup>1</sup>, P. Pelleau<sup>1</sup>, C. Prunier<sup>7</sup>, M. Roudaut<sup>1</sup>, L. Morvan<sup>1</sup>, D. Pierre<sup>1</sup>, E. Boisson<sup>1</sup>, M. Roudaut-Pitel<sup>1</sup>, I. Bernardo<sup>3</sup>, C. Corela<sup>3</sup>, J.L. Duarte<sup>3</sup>, M. De Lima<sup>8</sup>, L. Matias<sup>3</sup>, F. Farias<sup>5</sup>, R. Pellen<sup>1,6</sup>, B. Pereira<sup>5</sup>, C. Rigoti<sup>5</sup> & W. Roest<sup>1</sup>.

#### CRediT authorship contribution statement

**Philippe Schnürle:** Writing – original draft, Investigation.

#### Declaration of competing interest

The authors declare that they have no known competing financial interests or personal relationships that could have appeared to influence the work reported in this paper.

#### Data availability

Data will be made available on request.

#### Acknowledgments

We thank the captain, crew, and MCS technical team of the R/V Pourquoi-Pas? We also thank the OBS technical team who maintain and

constantly improve our OBS pool, as well as the land stations deployment team from Brazil and Portugal. This research was funded by Petrobras (Brazil) and Ifremer (France). The dataset collected during the MAGIC experiment is protected under a partnership with Petrobras. Any request has to be addressed to Daniel Aslanian ([aslanian@ifremer.fr](mailto:aslanian@ifremer.fr)) and Adriano Viana ([aviana@petrobras.com.br](mailto:aviana@petrobras.com.br)). R. Fuck acknowledges CNPq research fellowship. The authors acknowledge financial support from CAPES-COFEUCUB. The GMT (Wessel and Smith, 1998), Seismic Unix (Stockwell 1999; Cohen and Stockwell, 2003), and Geocluster (CGG-Veritas) software packages were used extensively in the redaction of this study.

## References

- Andrade, J.F.P., Gomes, M.P., Bezerra, F.H.R., de Castro, D.L., Vital, H., 2018. Morphotectonic development of the Ceará Terrace: a marginal ridge on the western side of the Romanche fracture zone in the Brazilian equatorial margin. *Geo Mar. Lett.* 38 (4), 371–384.
- Antobreh, A.A., Faleide, J.I., Tsikalas, F.T., Planke, S., 2009. Rift–shear architecture and tectonic development of the Ghana margin deduced from multichannel seismic reflection and potential field data. *Mar. Petrol. Geol.* 26 (3), 345–368.
- Aslanian, D., Gallais, F., Afilhado, A., Schnürle, P., Moulin, M., Evain, M., Dias, N., Soares, J., Fuck, R., da Cruz Pessoa Neto, O., Cupertino, J.A., Viana, A., the MAGIC Team, 2021. Deep structure of the Pará maranhão/barreirinhas passive margin in the equatorial Atlantic (NE Brazil). *J. S. Am. Earth Sci.* 110 <https://doi.org/10.1016/j.jsames.2021.103322>.
- Attoh, K., Brown, L., Guo, J., Heanlein, J., 2004. Seismic stratigraphic record of transpression and uplift on the Romanche transform margin, offshore Ghana. *Tectonophysics* 378 (1–2), 1–16.
- Basile, C., Mascle, J., Guiraud, R., 2005. Phanerozoic geological evolution of the Equatorial Atlantic domain. *J. Afr. Earth Sci.* 43, 275–282.
- Bonatti, E., Raznitsin, Y., Bortoluzzi, G., Boudillon, F., 1991. Geological studies of the eastern part of the Romanche transform (equatorial Atlantic): a first report. *Giorn. Geol.* 53 (2), 31–48.
- Campan, A., 1995. Analyse cinématique de l'Atlantique Equatorial, implications sur l'évolution de l'Atlantique Sud et sur la frontalière de plaque Amérique du Nord/Amérique du Sud. Université Pierre et Marie Curie, Paris, p. 352. Paris vol. I.
- de Castro, D.L., de Oliveira, D.C., Herrera, D.R.H., Bezerra, F.H.R., Romero, M.A.T., de Araújo, M.N.C., 2022. Crustal evolution of divergent and transform segments of the Brazilian Equatorial Margin derived from integrated geophysical data: insights from basement grain heritage. *Earth Sci. Rev.*, 104132 <https://doi.org/10.1016/j.earscirev.2022.104132>.
- Christensen, N.I., Mooney, W.D., 1995. Seismic velocity structure and composition of the continental crust: a global view. *J. Geophys. Res.* 100, 9761. <https://doi.org/10.1029/95JB00259>.
- Cohen, J.K., Stockwell Jr., J.W., 2003. CWP/SU: Seismic Unix Release 37: an Open Source Package for Seismic Research and Processing. Center for Wave Phenomena, Colorado School of Mines.
- Davison, I., Faull, T., Greenhalgh, J., Beirne, E.O., Steel, L., 2015. Transpressional Structures and Hydrocarbon Potential along the Romanche Fracture Zone: a Review, vol. 431. Geological Society, London, Special Publications, pp. 10–1144. SP431.2.
- Edwards, R.A., Whitmarsh, R.B., Scrutton, R.A., 1997. Synthesis of the crustal structure of the transform continental margin off Ghana, northern Gulf of Guinea. *Geo Mar. Lett.* 17, 12–20.
- Francheteau, J., Le Pichon, X., 1972. Marginal fracture zones as structural framework of continental margins in south Atlantic Ocean. *American Association of Petroleum Geologists* 56 (6), 991–1007.
- Gillard, M., Sauter, D., Tugend, J., Tomasi, S., Epin, M.E., Manatschal, G., 2017. Birth of an oceanic spreading center at a magma-poor rift system. *Sci. Rep.* 7.
- Gonçalves, S., Schnürle, P., Rabineau, M., Afilhado, A., Aslanian, D., Evain, M., Moulin, M., Loureiro, A., & Dias, N. Deep crustal structures with Reverse Time Migration applied to offshore wide-angle seismic data: equatorial and North-West Brazilian Margins; *J. S. Am. Earth Sci.*ences, (this issue).
- Gorini, M., 1977. The Tectonic Fabric of the Equatorial Atlantic and Adjoining Continental Margins. Ph.D. Thesis. Columbia University.
- Krueger, A., Murphy, M., Gilbert, E., Burke, K., 2012. Deposition and deformation in the deepwater sediment of the offshore Barreirinhas Basin, Brazil. *Geosphere* 8 (6), 1606–1631.
- Kusznir, N.J., Roberts, A.M., Alvey, A.D., 2018. Crustal structure of the conjugate Equatorial Atlantic Margins, derived by gravity anomaly inversion. In: McClay, K., Hammerstein, J. (Eds.), *Passive Margins: Tectonic, Sedimentation and Magmatism*. The Geological Society, London, Special Publication, 476. <https://doi.org/10.1144/SP476.5>.
- Kutu, J.M., 2013. Seismic and tectonic correspondence of major earthquake regions in southern Ghana with mid-atlantic transform-fracture zones. *Int. J. Geosci.* 4, 41164 <https://doi.org/10.4236/ijg.2013.410128> (Article ID).
- de Lima, M.V.A., Berrocal, J., Soares, J.E., Fuck, R.A., 2015. Deep seismic refraction experiment in northeast Brazil: new constraints for Borborema province evolution. *J. S. Am. Earth Sci.* 58, 335–349.
- Ludwig, W.J., Nafe, J.E., Drake, C.L., 1970. In: Maxwell, A.E. (Ed.), *Seismic Refraction, in the Sea*, vol. 4. Wiley, New York, pp. 53–84.
- Lutter, W.J., Nowack, R.L., 1990. Inversion for crustal structure using reflections of the PASSCAL Ouachita experiment. *Geophys. J. Int.* 95, 4633–4646.
- de Matos, R.M., Brown, L.D., 1992. Deep seismic profile of the Amazonian craton (northern Brazil). *Tectonics* 11 (3), 621–633.
- de Matos, R.M.D., Krueger, A., Norton, I., Casey, K., 2021. The fundamental role of the Borborema and Benin–Nigeria provinces of NE Brazil and NW Africa during the development of the South Atlantic cretaceous rift system. *Mar. Petrol. Geol.* 127, 104872.
- Moulin, M., Aslanian, D., Unternehr, P., 2010. A new starting point for the south and equatorial Atlantic ocean. *Earth Sci. Rev.* 98, 1–37.
- Moulin, M., Schnürle, P., Afilhado, A., Gallais, F., Dias, N., Evain, M., MAGIC Team., 2021. Imaging early oceanic crust spreading in the equatorial Atlantic Ocean: insights from the MAGIC wide-angle experiment. *J. S. Am. Earth Sci.* 111, 103493.
- Pavlis, N.K., Holmes, S.A., Kenyon, S.C., Factor, J.K., 2012. The development and evaluation of the earth gravitational model 2008 (EGM2008). *J. Geophys. Res. Solid Earth* 117 (B4).
- Sage, F., Pontoise, B., Mascle, J., Basile, C., Arnould, L., 1997. Crustal structure and ocean–continent transition at marginal ridge: the Côte d'Ivoire–Ghana marginal ridge. *Geo Mar. Lett.* 17, 40–48.
- Scarselli, N., Duval, G., Martin, J., McClay, K., Toothill, S., 2020. Insights into the early evolution of the Côte d'Ivoire margin (west Africa). Geological Society, London, Special Publications 476 (1), 109–133.
- Sandwell, D.T., Smith, W.H.F., 2009. Global marine gravity from retracked Geosat and ERS-1 altimetry: ridge segmentation versus spreading rate. *J. Geophys. Res.* 114 (B-1), B01411 <https://doi.org/10.1029/2008JB006008>.
- Stockwell Jr., J.W., 1999. The CWP/SU: seismic Unix package. *Comput. Geosci.* 25 (4), 415–419. [https://doi.org/10.1016/S0098-3004\(98\)00145-9](https://doi.org/10.1016/S0098-3004(98)00145-9).
- Tamara, J., McClay, K.R., Hodgson, N., 2020. Crustal structure of the central sector of the NE Brazilian equatorial margin. Geological Society, London, Special Publications 476 (1), 163–191.
- Tavares, A.C., de Castro, D.L., Bezerra, F.H.R., Oliveira, D.C., Vannucchi, P., Iacopini, D., Jovane, L., Vital, H., 2020. The Romanche fracture zone influences the segmentation of the equatorial margin of Brazil. *J. S. Am. Earth Sci.* 103 <https://doi.org/10.1016/j.jsames.2020.102738>.
- Wessel, P., Smith, W.H.F., 1998. New, improved version of the Generic Mapping Tools released. *Eos Trans. AGU* 79 (47), 579.
- White, R.S., McKenzie, D., O'Nions, R.K., 1992. Oceanic crustal thickness from seismic measurements and rare earth element inversions. *J. Geophys. Res.* 97, 19683–19715. <https://doi.org/10.1029/92JB01749>.
- Zalan, P.V., 2015. Re-interpretation of an ultra-deep seismic section in the pará-maranhão basin - implications for the petroleum potential of the ultra-deep waters. Offshore Technology Conference, Rio de Janeiro, Brazil, 26134, 27–29 October 2015.
- Zelt, C.A., 1999. Modelling strategies and model assessment for wide-angle seismic traveltimes data. *Geophys. J. Int.* 183–204.
- Zelt, C.A., Forsyth, D.A., 1994. Modeling wide-angle seismic data for crustal structure: southeastern Grenville Province. *J. Geophys. Res. Solid Earth* 99 (B6), 11687–11704.
- Zelt, C.A., Smith, R.B., 1992. Seismic travel time inversion for 2-D crustal velocity structure. *Geophys. J. Int.* 108, 16–34.